Design and synthesis of metal-based chemotherapeutic agents for targeted DNA interactions or DNA repair pathway modulation

Griend, C.J. van de

Chapter 2

pH dependence and structure-activity relationship for square planar Pt(II) and Pd(II) tetrapyridyl complexes interacting with DNA

Corjan van de Griend, Chucky Chau, Chantal Huisman, Lars Mensink, Maxime A. Siegler, Remus T. Dame, Sylvestre Bonnet.

Abstract

The interaction between metal complexes and DNA has been an important research field since the discovery of cisplatin. Here, we report the synthesis of a series of derivatives of the 6,6'-bis(2"-aminopyridyl)-2,2'-bipyridine (H_2babpby) ligand scaffold where either the terminal pyridyl groups have been functionalized with a methyl, methoxy, chloride, or trifluoromethyl substituent, or where the amine bridges have been replaced by thioether, ether, methylene, or carbonyl bridges. These 14 ligands were reacted with palladium(II) and platinum(II) salts to afford a series of 24 tetrapyridyl metal complexes that were all characterized in the solid state by crystal structure determination and elemental analysis, and in solution by NMR, mass spectrometry, and UV-vis spectroscopy. Remarkably, in aqueous solution the complexes containing NH or CH_2 bridges are easily deprotonated, which allowed their acidity constants (pK_a) to be determined. Overall, the palladium complexes have a 1-unit higher pK_a value, than their platinum analogues. The influence of the methyl groups and the electron-donating groups on the pK_a value is minimal, while the electron-withdrawing CF_3 groups resulted in a larger decrease by 2 pK_a units. Agarose gel electrophoresis showed pH- and ligand-dependent interactions between the metal complexes and plasmid DNA, but also several false negative interactions probably resulting from the dissociation of some of the intercalating metal complexes from the DNA during electrophoresis. Calf thymus DNA titration in solution and binding constant determination confirmed intercalation as the binding mode for most of these complexes at pH 4.5-5.0, as hypochromism and bathochromic shifts were observed with increasing DNA concentrations. At pH 8.0, titration of complexes containing an NH or CH_2 bridge with DNA showed that two reactions were taking place: first protonation, and second, binding to DNA. At high DNA concentration, the UV-vis spectra were identical to those obtained at pH 5. The lack of any absorbance above 450 nm for these spectra indicates that the metal complexes are fully protonated once fully bound to DNA. Titrations at pH 8 of compounds characterized by a low pK_a showed no significant interactions with DNA, highlighting the crucial role of the protonation state of the metal complexes for DNA intercalation: only the bicationic, fully protonated species interact significantly with double-stranded DNA.

2.1 Introduction

The discovery of the cytotoxic properties of cisplatin in 1965 by Rosenberg *et al.*[1] kickstarted the field of bioinorganic chemistry and ever since has inspired a myriad of studies exploring the interactions between inorganic compounds and their biological targets. The mechanism of action of cisplatin has been widely studied and the cytotoxicity of cisplatin is primarily induced by the crosslinking of DNA, which is an especially toxic type of DNA damage resulting in cell death upon accumulation.[2,3] Despite the early clinical successes of cisplatin and its widespread use in clinics

around the world, the treatment is plagued by side effects such as nephrotoxicity, neurotoxicity and platinum resistance,[4] underlining the necessity for the development of chemotherapy treatments with increased selectivity. Cisplatin analogues carboplatin and oxaliplatin were developed with reduced side effects but their application is limited by low efficacy.[5,6]

Since then, a large variety of metal complexes has been prepared and their interaction with DNA has been well documented.[7–10] A particularly interesting group of compounds are chemically stable, square-planar Pt(II)-tetrapyridyl compounds characterized by a stable 16 electron configuration.[11–13] Unlike cisplatin, the cytotoxicity mechanism of which relies on the hydrolysis of the chlorido ligands to facilitate the formation of crosslinks to DNA, chemically stable planar Pt(II) compounds offer a different type of interactions with DNA, namely intercalation.[14] Intercalation occurs when a planar aromatic system (at least) partly inserts between consecutive base pairs of double-stranded DNA (dsDNA). This supramolecular interaction, which is usually stabilized by π-π interactions, typically leads to unwinding of the DNA helix. Well-studied intercalators are e.g. ethidium bromide,[15] which is used in biochemistry to visualize DNA, and the metal complex $[Ru(bpy)_2(dppz)]^{2+}$ (bpy = 2,2'-bipyridine, dppz = dipyridophenazine),[16] which is well known for its "light switch" effect consisting in showing improved luminescence upon intercalation into DNA, while in the absence of DNA, the complex is not luminescent at all. Several factors can influence the intercalation of chemical compounds into DNA, including their size,[17] the pH and the protonation state of the intercalator,[18] their charge,[19] and overall the electrostatic interactions.[20]

DNA, however, can adopt multiple structures, and other non-canonical foldings, such as G-quadruplexes[21–23], 3-way junctions[24,25] and 4-way junctions, have been extensively characterized. We recently reported the high toxicity of the square-planar platinum(II) compound $[Pt(H_2bapbpy)]^{2+}$, where H_2bapbpy = 6,6'-bis(2"-aminopyridyl)-2,2'-bipyridine. In this study, a crystal structure of this complex interacting with a small palindromic DNA oligomer 5'-d(CGTACG)-3 was obtained. In this crystal structure, the DNA formed a 4WJ-like motif, with the metal complex binding at its core[26]. It was further observed that the bridging nitrogen group of the H_2bapbpy ligand became acidic upon coordination of the tetrapyridyl ligand to the metal. Deprotonation leads to a reduced overall charge of the complex, which possibly influences its interactions with DNA. En route to studying such interaction in more details, we realized that the interaction of this family of helical metal complexes with standard double-stranded DNA, and the role of NH bridge deprotonation on it, were essentially unknown, which precluded more intricate studies with 4WJ DNA.

Here, we engaged in a systematic study of the interaction between $[M^{II}(H_2L)]^{2+}$ metal complexes and double-stranded DNA, where H_2L is a H_2bapbpy-like tetrapyridyl ligand and M is a square-planar d^8 transition metal center (M = Pd(II) or Pt(II)). In particular, we explored the pivotal role of pH in this interaction by playing with the electron-

richness of the H_2L ligand. To do so, we synthesized three series of H_2bapbpy (H_2**L1**) derivatives, including: H_2**L2-5,** containing a methyl group at various positions on the terminal pyridine; H_2**L6-9,** that were functionalized with electron-donating (methoxy for H_2**L6**) or electron-withdrawing (chloride for H_2**L7**, trifluoromethyl for H_2**L8**) groups at the *para* position of the terminal pyridines, or where the terminal pyridyl groups were replaced by quinolyl group (H_2**L9**); and H_2**L10-14**, in which the two NH bridges of the ligand were changed into methylamine (H_2**L10**), thioether (H_2**L11**), carbonyl (H_2**L12**), methylene (H_2**L13**), or ether bridges (H_2**L14**, see Scheme 1). These ligands were coordinated to Pd(II) or Pt(II); the 24 metal complexes were fully characterized both in the solid state and in solution. The first pK_a values of all acidic complexes that could be deprotonated were determined. Then, the interaction of these complexes with calf thymus DNA was studied by plasmid agarose gel electrophorese and UV-vis titrations at varying pH. Furthermore, the binding constants of the metal complexes with calf thymus DNA were determined at pH 4.5, where all metal complexes were fully protonated. Finally, we discuss the structure-activity relationship of this series of metal complexes and their interactions with DNA.

2.2 Results

2.2.1 Synthesis

A series of 14 tetrapyridyl ligands was prepared as shown in Scheme 1 and detailed in the experimental part; all yields are recorded in Table 1. The first group of ligands was H_2bapbpy (H_2**L1**) and its symmetrical dimethylated analogues (H_2**L2-5**), for which all possible positions of the methyl groups on the terminal pyridines were investigated. These ligands were synthesized by a Buchwald-Hartwig cross-coupling reaction between 6,6'-dibromo-2,2'-dipyridyl (Br_2bpy) and 2-aminopyridine derivatives, as reported in the literature.[26,27] The second set of ligands had either an electron-donating or an electron-withdrawing group in *para* position to the imine nitrogen on the terminal pyridines, which maximizes, in principle, the electronic effect of the substituent on the coordinated metal center. Ligands H_2**L6-7** bore methoxide or chloride electron-donating groups; they were synthesized by an adapted Buchwald-Hartwig procedure, and obtained in 49% and 67% yield, respectively. These reaction conditions proved insufficient when the electron-withdrawing trifluoromethyl group was present on the 2-aminopyridine moiety. This problem was circumvented by placing the trifluoromethyl group on the bromo moiety instead of on the amino moiety. Ligand H_2**L8** was hence achieved in two steps: First, a reported nucleophilic aromatic substitution of 6,6'-dibromo-2,2'-bipyridine to afford 6,6'-diamino-2,2'-bipyridine[28], followed by a Buchwald-Hartwig cross-coupling reaction of the latter with 2-bromo-4-(trifluoromethyl)pyridine, which afforded ligand H_2**L8** in 75% yield. Finally, a reported Buchwald-Hartwig cross-coupling reaction with 2-aminoquinoline afforded ligand H_2**L9**, which had an extended aromatic system.

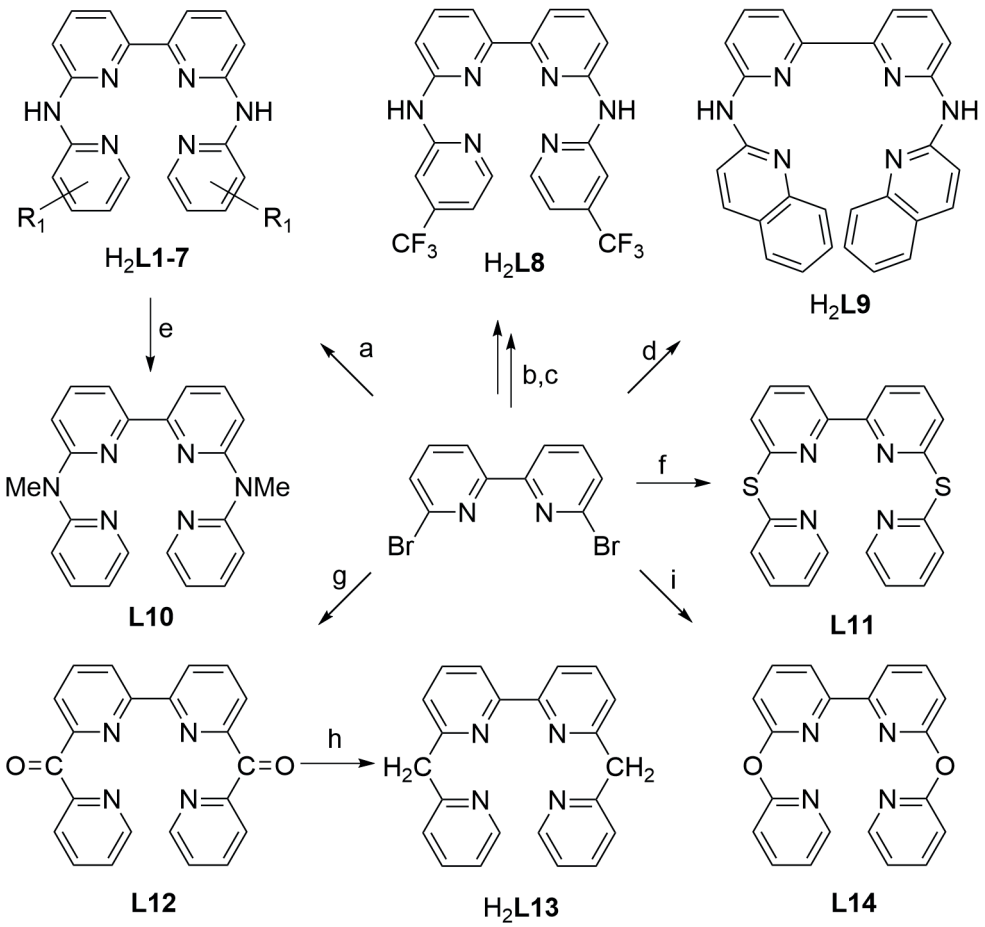

Scheme 1. Synthesis of tetrapyridyl ligands H2**L1**-**L14**. a) rac-BINAP, [Pd(dba)$_2$], KOtBu, 2-aminopyridine derivatives, toluene, 80 °C. b) K, NH_3, $Fe(NO_3)\cdot 9H_2O$, -78 °C KOH. c) rac-BINAP, [Pd(dba)$_2$], KOtBu, 2-bromo-4-(trifluoromethyl)pyridine, toluene, 80 °C. d) rac-BINAP, [Pd(dba)$_2$], KOtBu, 2-aminoquinoline, toluene, 80 °C. e) MeI, DMF, room temperature. f) 2-mercaptopyridine, KCO_3, DMF, 160 °C. g) n-BuLi (2.2 eq), THF, N-methoxy-N-methylpicolinamide, 95 °C, N_2 atmosphere. h) KOH, diethylene glycol, hydrazine, 250 °C. i) 2-hydroxypyridine, NaH, DMSO, 180 °C.

The final group of H_2bapbpy analogues consisted in ligands where the bridging NH group was replaced by a variety of other groups. First, in H_2**L10** the bridging amine was methylated by the reaction of H_2**L1** with an excess of MeI, to afford **L10** in 66% yield.[29] Next, the thioether analogue **L11** was synthesized in 45% yield by a nucleophilic aromatic substitution in DMF with potassium carbonate as a base.[30] The synthesis of ligand **L12**, which has two bridging carbonyl groups, was achieved in 33% yield *via* an adapted Weinreb ketone synthesis described in the literature.[31] A double Wolff-Kishner reduction of **L12** with hydrazine in diethylene glycol resulted in ligand H_2**L13** bearing two bridging methylene groups in 98% yield.[32] Finally, the bis-ether ligand **L14** was obtained in 75% yield by the nucleophilic substitutions of bromides in Br_2bpy with

two equivalents of deprotonated 2-hydroxypyridine.[33] The wide range of H_2bapbpy analogues reported here were all synthesized starting from Br_2bpy; they demonstrate the high synthetic versatility of this ligand scaffold notably for the study of structure-activity relationships.

Each H_2bapbpy-based ligand was then coordinated to platinum(II) and palladium(II) to afford $[M^{II}(H_2\mathbf{L1\text{-}10})]^{2+}$, $[M^{II}(\mathbf{L11\text{-}12})]^{2+}$, $[M^{II}(H_2\mathbf{L13})]^{2+}$ and $[M^{II}(\mathbf{L14})]^{2+}$ as chloride salts in yields ranging from 39 to 81%, as recorded in Table 2. The synthesis of most metal complexes was straightforward. Some of the metal complexes were acidic (see below); the most acidic complexes ($[M(H_2\mathbf{L1\text{-}9})]^{2+}$) could even be purified by silica gel column chromatography, provided the eluents contained 1 vol% triethylamine (see Experimental section). Special effort was made during the synthesis of the acidic complexes, capable of deprotonation, to isolate the final products in their fully protonated, bicationic state. This method allowed simpler characterization as a single species, and it increased water solubility. The palladium complexes [Pd(**L11**)] $(Cl)_2$ and [Pd(**L12**)]$(Cl)_2$ however, proved to be unstable in DMSO and insoluble in any other solvent system. This problem made it impossible to fully characterize these two compounds by NMR spectroscopy, as the ligand was partly substituted by DMSO-*d6* during the time scale of a ^{13}C NMR measurement. These two compounds were therefore not used for further investigations, and only a crystal structure (for $[Pd(\mathbf{L11})]^{2+}$) will be discussed below. Finally, a multitude of coordination reactions of the ether ligand **L14** to either metal precursors were tried, resulting steadfast in insoluble beige-colored solid substances that could not be analyzed or identified; therefore, the synthesis of the palladium and platinum complexes of this ligand was abandoned. In total, we report here the successful synthesis and full characterization of 12 novel platinum and 10 novel palladium novel complexes.

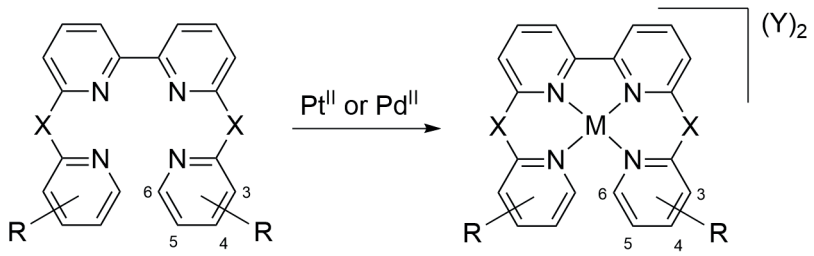

Scheme 2. Synthesis of metal complexes based on the $[Pd(H_2bapbpy]^{2+}$ and $[Pt(H_2bapbpy)]^{2+}$ scaffold by coordination of the tetrapyridyl ligands to $[Pd(cod)Cl_2]$ or $[Pt(MeCN)_2(Cl)_2]$, respectively. X = NH, S, O, C=O, or CH_2, see text

Table 1. Preparative yields for the coordination reaction shown in scheme 2.

Ligand	Bridging group	R	Synthetic yield (%)	
			Pt complex	Pd complex
H_2**L1**	NH	H	-	-
H_2**L2**	NH	3-Me	68	66
H_2**L3**	NH	4-Me	60	71
H_2**L4**	NH	5-Me	70	57
H_2**L5**	NH	6-Me	67	40
H_2**L6**	NH	4-OMe	40	52
H_2**L7**	NH	4-Cl	48	41
H_2**L8**	NH	4-CF_3	60	36
H_2**L9**	NH	[a]	64	51
L10	*N*-Me	H	39	71
L11	S	H	71	50
L12	C=O	H	45	43
H_2**L13**	CH_2	H	55	81
L14	O	H	-	-

[a] in H_2**L9** the terminal pyridyl groups have been replaced by 2-quinolyl groups.
[b] All metal complexes were isolated in their bis-protonated and bicationic form.

2.2.2 Crystal structures

Crystals suitable for X-ray analysis were obtained for all isolated metal complexes, except for [Pd(**L12**)]$(Cl)_2$, which was unstable. The crystal structure of complex [Pd(**L2**)] was the only one to show full deprotonation, and all other structures showed the fully protonated bicationic metal complexes. This large library of crystals was grown by vapor diffusion using a single drop of acid, such as triflic acid, HPF_6, $HClO_4$, or HBF_4, to keep the metal complex protonated (0.2 mg/mL). This method also led to counter-anion exchange, and the native chloride cation of the isolated powder compounds was usually replaced, in the crystal structures, by the acid anion. All 12 platinum crystal structures are shown in figures 1, 2 and the palladium compounds in figures 3, 4.

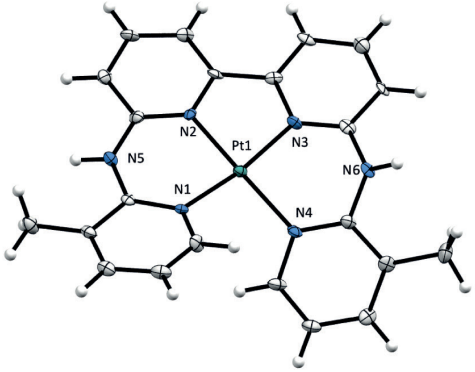

$[Pt(H_2\mathbf{L2})]^{2+}$

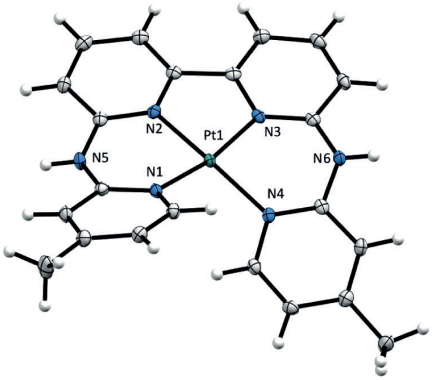

$[Pt(H_2\mathbf{L3})]^{2+}$

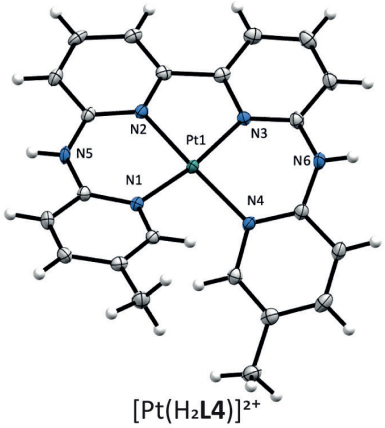

$[Pt(H_2\mathbf{L4})]^{2+}$

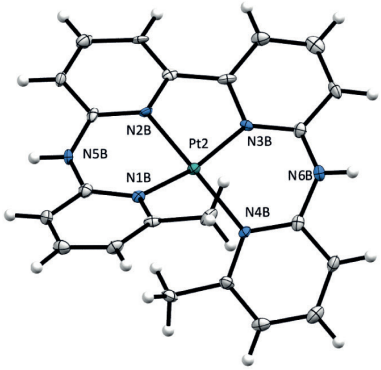

$[Pt(H_2\mathbf{L5})]^{2+}$

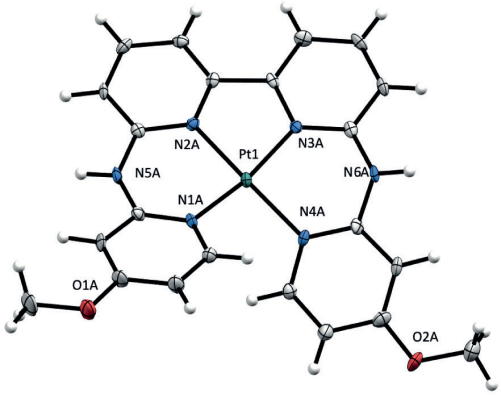

$[Pt(H_2\mathbf{L6})]^{2+}$

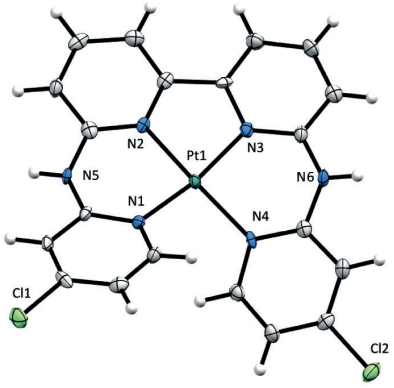

$[Pt(H_2\mathbf{L7})]^{2+}$

Figure 1. Displacement ellipsoid plots (50% probability level) for the bicationic part of the x-ray crystal structures for $[Pt(H_2\mathbf{L2})](OTf)_2$, $[Pt(H_2\mathbf{L3})](OTf)_2 \bullet (MeOH)_2$, $[Pt(H_2\mathbf{L4})](OTf)_2$, $[Pt(H_2\mathbf{L5})](OTf)_2$, $[Pt(H_2\mathbf{L6})](OTf)_2$, $[Pt(H_2\mathbf{L7})](OTf)_2$ at 110(2) K. Counter ions and solvent molecules have been omitted for clarity.

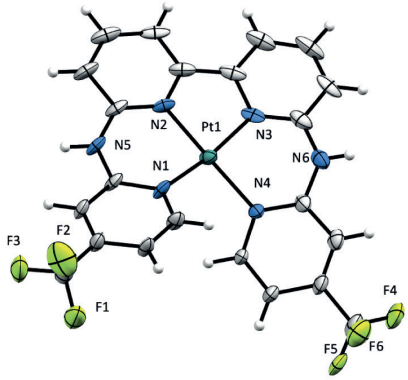

$[Pt(H_2\mathbf{L8})]^{2+}$

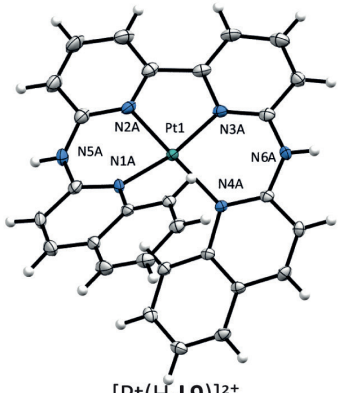

$[Pt(H_2\mathbf{L9})]^{2+}$

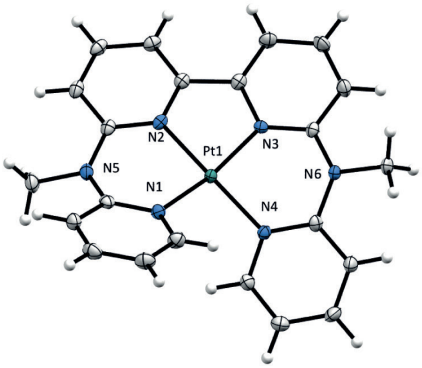

$[Pt(\mathbf{L10})]^{2+}$

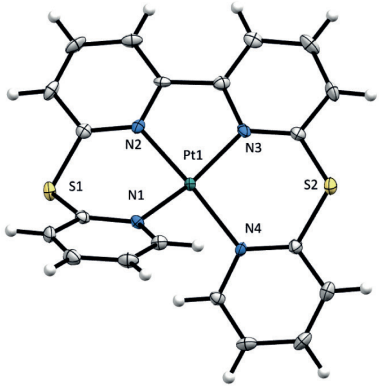

$[Pt(\mathbf{L11})]^{2+}$

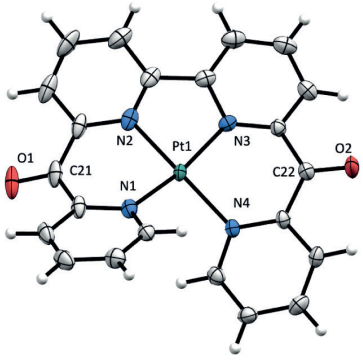

$[Pt(\mathbf{L12})]^{2+}$

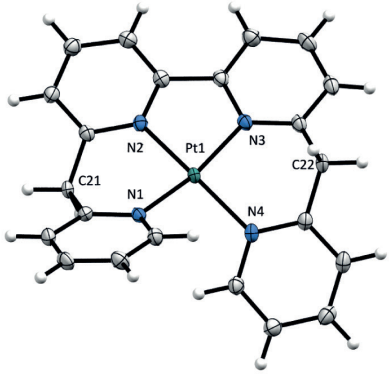

$[Pt(H_2\mathbf{L13})]^{2+}$

Figure 2. Displacement ellipsoid plots (50% probability level) for the bicationic part of the x-ray crystal structures for $[[Pt(H_2\mathbf{L8})](OTf)_2 \bullet MeOH$, $[Pt(H_2\mathbf{L9})](OTf)_2$, $[Pt(\mathbf{L10})](OTf)_2 \bullet DCM$, $[Pt(\mathbf{L11})](PF_6)_2 \bullet MeCN$, $[Pt(\mathbf{L12})][Pt(DMSO)(Cl)_3]_2 \bullet CHCl_3$, $[Pt(H_2\mathbf{L13})](PF_6)_2$ at 110(2) K. Counter ions and solvent molecules have been omitted for clarity.

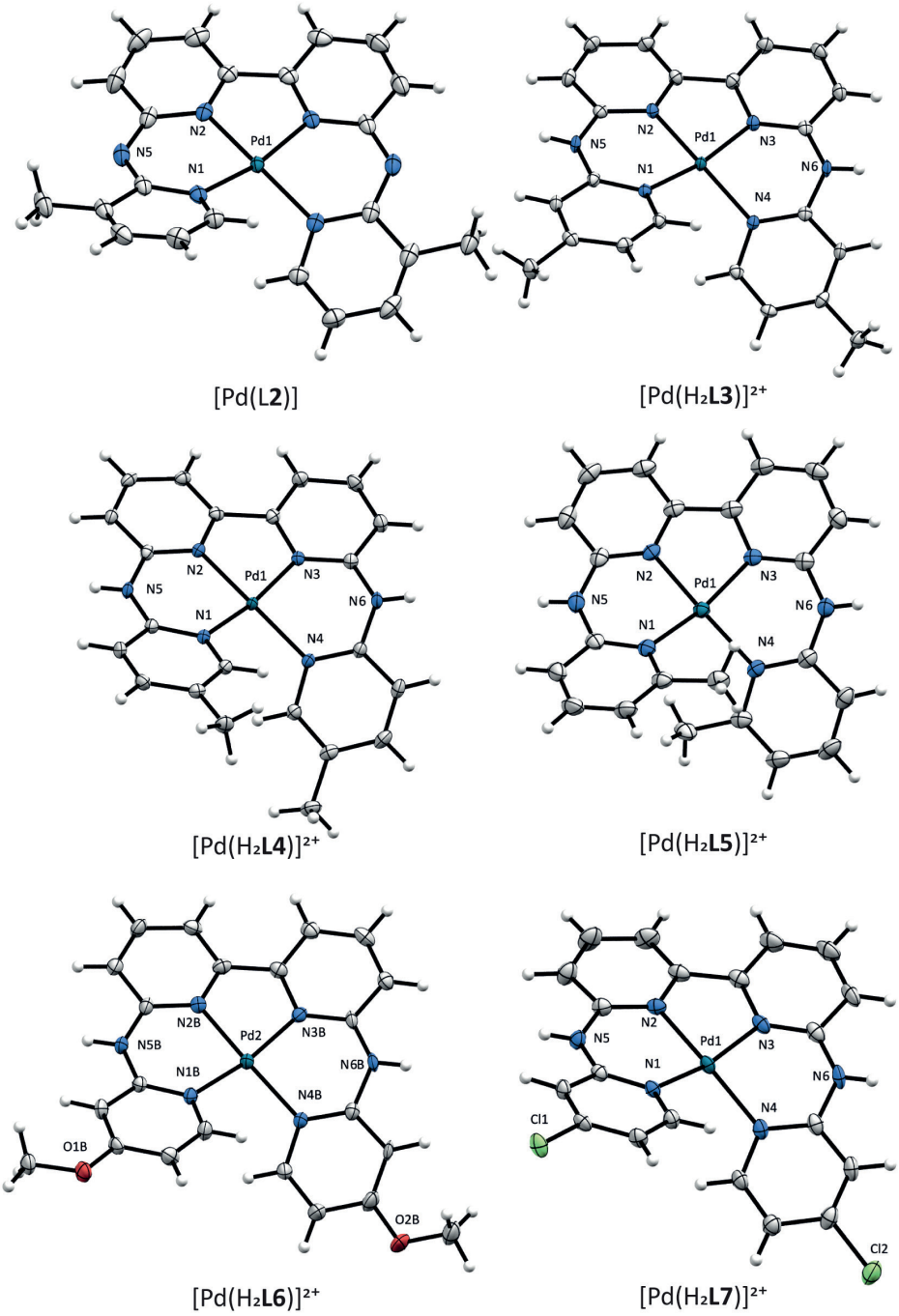

Figure 3. Displacement ellipsoid plots (50% probability level) for [Pd(**L2**)], [Pd(H_2**L3**)](Cl)(BPh_3), [Pd(H_2**L4**)]($OTf)_2$, [Pd(H_2**L5**)](BF_4)(H_2O), [Pd(H_2**L6**)]($OTf)_2$MeCN, [Pd(H_2**L7**)]($OTf)_2$ at 110(2) K. Counter ions and solvent molecules have been omitted for clarity.

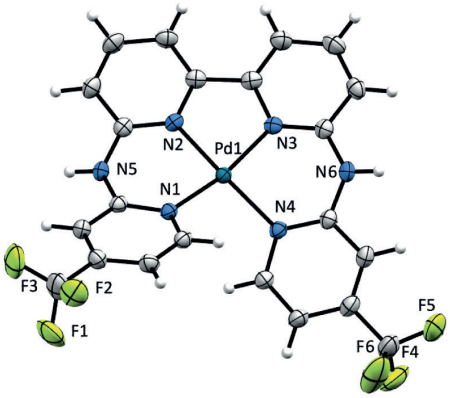

$[Pd(H_2\mathbf{L8})]^{2+}$

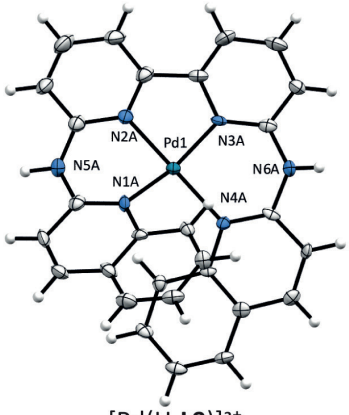

$[Pd(H_2\mathbf{L9})]^{2+}$

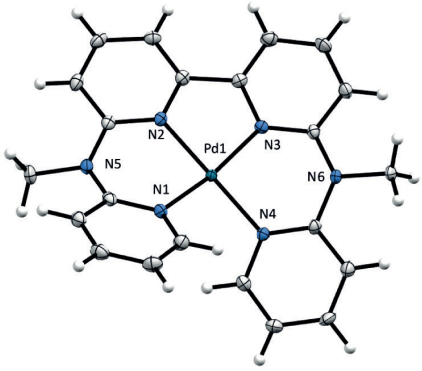

$[Pd(\mathbf{L10})]^{2+}$

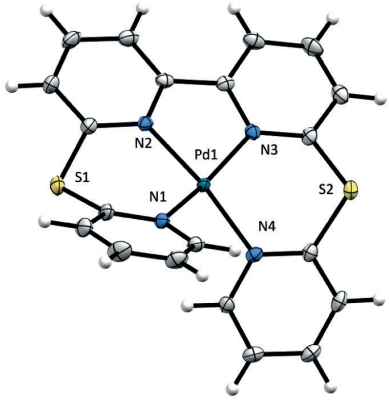

$[Pd(\mathbf{L11})]^{2+}$

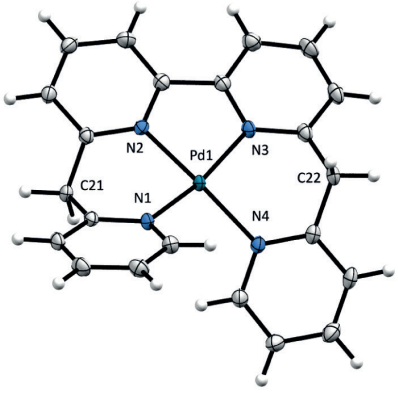

$[Pd(H_2\mathbf{L13})]^{2+}$

Figure S4. Displacement ellipsoid plots (50% probability level) for $[Pd(H_2\mathbf{L8})](OTf)_2(H_2O)_3$, $[Pd(H_2\mathbf{L9})](OTf)_2$, $[Pd(\mathbf{L10})](OTf)_2DCM$, $[Pd(\mathbf{L11})](PF_6)_2DCM$, and $[Pd(H_2\mathbf{L13})](PF_6)_2$ at 110(2) K. Counter ions and solvent molecules have been omitted for clarity.

Table 2. Selected bond distances (Å) and angles (°) in the crystal structures of complexes $[M(H_2\mathbf{L2\text{-}13})]^{2+}$.

Compound	$[Pt(H_2\mathbf{L2})]^{2+}$	$[Pt(H_2\mathbf{L3})]^{2+}$	$[Pt(H_2\mathbf{L4})]^{2+}$	$[Pt(H_2\mathbf{L5})]^{2+}$ [c]	$[Pt(H_2\mathbf{L6})]^{2+}$ [b]	$[Pt(H_2\mathbf{L7})]^{2+}$	$[Pt(H_2\mathbf{L8})]^{2+}$	$[Pt(H_2\mathbf{L9})]^{2+}$ [d]	$[Pt(\mathbf{L10})]^{2+}$	$[Pt(\mathbf{L11})]^{2+}$	$Pt(\mathbf{L12})]^{2}$	$[Pd(H_2\mathbf{L13})]^{2+}$
M-N1	2.2023(7)	2.025(2)	2.029(2)	2.022(4)	2.007(5)	2.033(5)	2.01(1)	2.034(2)	2.014(2)	2.033(5)	2.033(4)	1.988(2)
M-N2	2.001(5)	1.984(1)	1.991(2)	1.982(5)	1.983(6)	1.979(5)	1.98(1)	1.972(3)	1.982(2)	2.001(5)	1.997(4)	2.030(2)
M-N3	1.986(8)	1.990(2)	1.982(2)	1.970(5)	1.991(5)	1.980(5)	1.97(1)	1.972(2)	1.979(2)	2.014(5)	1.996(4)	1.999(2)
M-N4	2.031(5)	2.025(1)	2.026(2)	2.034(4)	2.011(6)	2.022(5)	2.04(1)	2.032(3)	2.012(2)	2.036(5)	2.038(4)	2.033(2)
X1-C5	1.391(9)	1.384(2)	1.384(3)	1.388(8)	1.374(9)	1.360(8)	1.3(7)	1.371(5)	1.404(3)	1.750(7)	1.493(8)	1.501(5)
X1-C6	1.37(1)	1.367(3)	1.368(3)	1.383(8)	1.384(8)	1.372(8)	1.36(2)	1.367(5)	1.386(3)	1.757(6)	1.496(8)	1.506(4)
X2-C15	1.380(9)	1.370(2)	1.379(4)	1.387(7)	1.374(9)	1.383(8)	1.39(2)	1.371(5)	1.377(3)	1.751(7)	1.507(7)	1.508(5)
X2-C16	1.39(1)	1.385(3)	1.378(3)	1.380(7)	1.371(8)	1.359(8)	1.36(2)	1.375(4)	1.400(3)	1.760(7)	1.500(7)	1.495(4)
C5-X1-C6	132.4(7)	130.5(8)	133.3(2)	131.3(3)	132.2(2)	131.7(0)	132.9(8)	131.7(3)	126.6(5)	106.3(4)	122.6(1)	117.5(2)
C15-X2-C16	128.1(7)	131.0(5)	130.1(7)	134.6(1)	132.0(0)	132.5(7)	132.0(2)	132.6(3)	126.7(3)	107.1(9)	125.5(7)	118.7(3)
N1-M-N3	169.3(3)	168.(2)	169.(8)	163.0(6)	169.1(6)	167.7(8)	168.(3)	166.1(1)	164.8(1)	161.5(6)	165.(8)	166.4(1)
N2-M-N4	165.0(3)	167.7(1)	167.5(1)	165.3(4)	167.0(7)	168.2(6)	167.1(3)	165.8(1)	166.0(2)	162.(9)	171.1(4)	166.5(1)
τ_4	0.182	0.171	0.161	0.224	0.169	0.170	0.174	0.199	0.207	0.252	0.164	0.192
helicity	15.9(6)	14.5(8)	14.1(3)	20.4(9)	14.6(9)	14.6(7)	14.5(7)	17.9(1))	18.9(8)	23.6(2)	14.6(8)	17.4(7)

Table 2. Selected bond distances (Å) and angles (°) in the crystal structures of complexes $[M(H_2\mathbf{L2\text{-}13})]^{2+}$.

Compound	[Pd(**L2**)]	$[Pd(H_2\mathbf{L3})]^{2+}$	$[Pd(H_2\mathbf{L4})]^{2+}$	$[Pd(H_2\mathbf{L5})]^{2+}$	$[Pd(H_2\mathbf{L6})]^{2+}$ [c]	$[Pd(H_2\mathbf{L7})]^{2+}$	$[Pd(H_2\mathbf{L8})]^{2+}$	$[Pd(H_2\mathbf{L9})]^{2+}$ [d]	$[Pd(\mathbf{L10})]^{2+}$	$[Pd(\mathbf{L11})]^{2+}$	$Pd(\mathbf{L12})]^{2+}$	$[Pd(H_2\mathbf{L13})]^{2+}$
M-N1	2.03(0)	2.034(2)	2.037(1)	2.050(2)	2.035(4)	2.034(2)	2.033(2)	2.035(3)	2.016(2)	2.038(2)	n.d.	2.034(2)
M-N2	1.97(5)	1.978(2)	1.987(2)	1.983(2)	1.990(4)	1.986(2)	1.981(2)	1.961(5)	1.982(2)	2.015(2)	n.d.	1.995(2)
M-N3	1.97(5)	1.982(2)	1.981(1)	1.984(2)	1.980(4)	1.983(2)	1.986(2)	1.970(4)	1.977(2)	2.007(2)	n.d.	2.001(2)
M-N4	2.03(0)	2.035(2)	2.036(2)	2.061(2)	2.038(4)	2.029(2)	2.037(2)	2.046(4)	2.017(2)	2.036(2)	n.d.	2.042(2)
X1-C5	1.338(2)	1.377(3)	1.383(2)	1.380(3)	1.392(7)	1.368(4)	1.378(3)	1.367(8)	1.405(3)	1.763(3)	n.d.	1.498(4)
X1-C6	1.343(2)	1.366(3)	1.368(2)	1.369(3)	1.362(7)	1.371(4)	1.371(3)	1.373(8)	1.384(3)	1.760(3)	n.d.	1.509(3)
X2-C15	1.343(2)	1.373(3)	1.371(2)	1.369(3)	1.388(7)	1.367(4)	1.367(3)	1.369(8)	1.381(3)	1.756(3)	n.d.	1.510(3)
X2-C16	1.338(2)	1.373(3)	1.384(2)	1.380(3)	1.392(7)	1.378(4)	1.373(3)	1.365(6)	1.403(3)	1.752(3)	n.d.	1.497(3)
C5-X1-C6	126.3(8)	132.7(2)	130.1(7)	131.2(2)	131.3(4)	132.4(1)	128.5(2)	130.8(5)	126.7(9)	107.5(5)	n.d.	117.0(3)
C15-X2-C16	126.3(8)	131.3(4)	132.6(0)	131.0(2)	130.9(0)	131.1(4)	132.3(2)	132.6(4)	126.2(0)	106.1(4)	n.d.	118.3(2)
N1-M-N3	166.7(8)	167.4(3)	167.9(7)	162.25(7)	165.9(2)	165.8(9)	165.23(8)	164.4(2)	167.7(8)	161.4(5)	n.d.	165.(3)
N2-M-N4	166.7(8)	166.0(7)	166.5(8)	162.87(7)	168.2(8)	165.7(5)	168.10(8)	164.3(2)	165.0(7)	161.4(7)	n.d.	165.9(1)
τ_4 [a]	0.188	0.188	0.180	0.247	0.183	0.201	0.189	0.222	0.193	0.263	n.d.	0.204
helicity	16.4(5)	16.6(4)	16.6(3)	22.7(3)	15.9(3)	18.0(8)	16.6(2)	20.3(1)	19.8(2)	24.7(2)	n.d.	18.6(7)

[a] The coordination angles N1-M1-N4 (α) and N3-M1-N6 (β)were used to calculate τ_4.[40] $\tau_4 = \frac{360 - (\alpha + \beta)}{141}$

[b] The structure consists of two crystallographically independent formula units. The bond distance and angles are given for molecule A.

[c] The structure consists of two crystallographically independent formula units. The bond distance and angles are given for molecule B.

[d] The structure consists of four crystallographically independent formula units. The bond distance and angles are given for molecule A.

n.d. = not determined.

Overall, the crystal structures of these metal compounds showed a great degree of similarity. The crystal lattices showed no metal-metal interaction as sometimes observed for palladium[34] or platinum[35] structures. All crystal structures showed a distorted, helical and chiral square-planar conformation induced by the steric clash between the *ortho* hydrogen atoms on the terminal pyridines of the ligand, which is in accordance with previously reported crystal structures of metal complexes based on this family of ligands.[26,27,36–39] In all structures both enantiomers are present due to an inversion center in the unit cell. The N1N3N4N6 dihedral angle was calculated as a measure of the helicity; the platinum compounds showed slightly smaller helicity than their palladium analogues. The modification of the pyridyl substituents in analogues $[M(H_2\mathbf{L2\text{-}8})]^{2+}$ did not result in significant changes to the distortion angle either, which generally was around 15° for platinum and 16° for the palladium compounds. Only $[M(H_2\mathbf{L5})]^{2+}$ deviated a bit from this value, as the steric clash between both *ortho* methyl groups significantly increased the distortion angles, compared to hydrogen atoms, to 20.4(9)° for $[Pt(H_2\mathbf{L5})]^{2+}$ and 22.7(3)° for $[Pd(H_2\mathbf{L5})]^{2+}$. This effect was also observed for complexes $[M(H_2\mathbf{L9})]^{2+}$ where the extended aromatic system forced an increased distortion, albeit to a smaller degree than for $[M(H_2\mathbf{L5})]^{2+}$ (17.9(1)° for $[Pt(H_2\mathbf{L9})]^{2+}$ and 20.3(1)° for $[Pd(H_2\mathbf{L9})]^{2+}$). Alterations of the bridging amine bridge showed consistently a more pronounced effect on the helicity of the ligand: methylation in complexes $[M(\mathbf{L10})]^{2+}$ resulted in a helicity angle of 18.9(8)° and 19.8(2)°, while the thioether complexes $[M(\mathbf{L11})]^{2+}$ showed an even larger increase of the helicity angle to 23.6(2)° and 24.7(2)° for platinum and palladium, respectively. Finally, the bridging methylene group in complexes $[M(H_2\mathbf{L13})]^{2+}$ showed a more subdued effect, with distortion angles of 17.4(7)° for $[Pt(H_2\mathbf{L13})]^{2+}$ and 18.6(7)° for $[Pd(H_2\mathbf{L13})]^{2+}$.

2.2.3 pK_a value determination

As mentioned previously, for non-methylated H_2bapbpy-based ligands, a proton of the bridging amine group becomes acidic upon coordination of the ligand to palladium(II) or platinum(II), and it can be deprotonated in basic solutions. The pK_a values of all metal complexes of this series were hence measured accurately, as pH is often a crucial parameter modulating the interaction between metallodrugs and biological molecules.[41] The determination of these pK_a values was performed using UV-vis spectroscopy and a titration protocol at constant ionic strength published by Martínez *et. al.*.[41] As mentioned above, all divalent metal compounds were isolated in their fully protonated, dicationic states $[M(H_2\mathbf{LX})]^{2+}$ with chloride counter anions. As a consequence, they were soluble in water. When the pH was increased during titration, all metal compound solutions showed clear changes by UV-vis spectroscopy, as can be seen for a representative example ($[Pt(H_2\mathbf{L1})]^{2+}$) in Figure 5. In all cases the presence of two clear isosbestic points indicated that only two distinct species were interconverting during titration: the fully protonated complex $[M(H_2\mathbf{L1X})]^{2+}$ and the monovalent

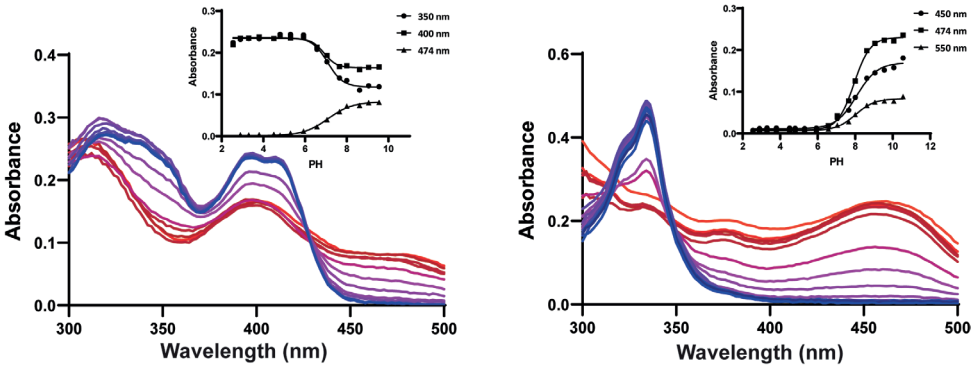

Figure 5. Absorption spectra at variable pH's for $[Pt(H_2\mathbf{L1})]^{2+}$ (left) and $[Pt(H_2\mathbf{L13})]^{2+}$ (right). The blue-to-red gradient represents color-coding of the pH of the solution, from acidic (pH 2.5) to basic (pH 11.0) conditions, respectively.

Table 3. pK_a values for the first deprotonation of $[M(H_2\mathbf{LX})]^{2+}$ complexes in aqueous solution, at T = 25 °C, ionic strength 0.1 M, (M = Pt^{II} and Pd^{II}).

			pK_a [a]					
Entry	Ligand	R	$M=Pt^{II}$			$M=Pd^{II}$		
1	$H_2\mathbf{L1}$	-	7.0	±	0.2	8.1	±	0.1
2	$H_2\mathbf{L2}$	3-Me	7.0	±	0.1	8.5	±	0.3
3	$H_2\mathbf{L3}$	4-Me	6.7	±	0.1	7.7	±	0.1
4	$H_2\mathbf{L4}$	5-Me	6.8	±	0.1	7.8	±	0.2
5	$H_2\mathbf{L5}$	6-Me	8.3	±	0.2	>8	±	-
6	$H_2\mathbf{L6}$	4-OMe	6.8	±	0.2	7.9	±	0.2
7	$H_2\mathbf{L7}$	4-Cl	5.8	±	0.1	7.1	±	0.1
8	$H_2\mathbf{L8}$	4-CF_3	5.1	±	0.1	6.3	±	0.1
9	$H_2\mathbf{L9}$	-	5.7	±	0.3	7.6	±	0.3
10	$H_2\mathbf{L13}$	-	7.9	±	0.1	8.5	±	0.1

[a] The 95% confidence interval on the pK_a values was based on 2 independent experiments and, for each experiment, on data fitting of Absorbance=f(pH) at 3 distinct wavelengths chosen for maximal variations in absorbance.

species $[M(H\mathbf{LX})]^+$. The spectroscopic spectra for all other compounds can be found in Appendix I figures SI.1-SI.20. In fact, these metal complexes can be deprotonated twice, as both bridging amines can be deprotonated, which is corroborated by the crystal structure of the neutral complex [Pd(**L2**)] described above. However, an orange-colored precipitate formed when titration was pursued to higher pH values, which was attributed to the hydrophobic character of the doubly deprotonated form of these metal complexes. In fact, all complexes afforded upon double deprotonation a neutral species, which exhibited dramatically reduced water solubility leading to precipitation, thus preventing the determination of the pK_a value corresponding to the second deprotonation event. However, the pK_a values associated with the first deprotonation

event could be determined precisely for all metal complexes in this series except for $[Pd(H_2\mathbf{L5})]^{2+}$, for which precipitation started during the first deprotonation step, as seen in figure SI.15. For this complex, only an broad estimation of the first pKa can be given ($pK_a > 8$).

In general, the pK_a values found for the palladium complexes are 1 pK_a unit higher than those found for their platinum analogues. The presence and the position of two methyl groups did not have a significant effect on the pK_a values, except for $[M(H_2\mathbf{L5})]^{2+}$, which showed a higher pK_a for both metals. This effect was attributed to the steric strain enforced by the *ortho* methyl groups, which may disfavor deprotonation. Indeed, the distorted ligand geometry deviated from a flat conformation, thus reducing the charge stabilization in the mono-deprotonated form resulting from charge delocalization over the aromatic system. Interestingly, the steric strain caused by the extension of the aromatic system to quinolyl groups in $[M(H_2(\mathbf{L9})]^{2+}$ resulted in the opposite result: the pK_a value was found lower in comparison with that of the bis-methylated metal compounds. The addition of electron-donating or electron-withdrawing groups showed diverse results. On the one hand, the methoxy substituents in $[M(H_2\mathbf{L6})]^{2+}$ led to similar pK_a values compared to the unsubstituted $[M(H_2\mathbf{L1})]^{2+}$, while the chloride substituents resulted in a decrease of pK_a values by 1 pK_a unit for $[M(H_2\mathbf{L7})]^{2+}$. A more pronounced effect was observed for the electron-withdrawing *para*-trifluoromethyl group in $[M(H_2\mathbf{L8})]^{2+}$, which showed a value that was 2 pK_a unit lower compared to $[M(H_2\mathbf{L1})]^{2+}$. As a note, it must be mentioned that the electron-donating and electron-withdrawing groups were located on the *para* position to the coordinated nitrogen atom, which is in principle optimal for inducing electronic effect on the metal center. Unexpectedly, the methylene-bridged complexes $[Pt(H_2\mathbf{L13})]^{2+}$ and $[Pd(H_2\mathbf{L13})]^{2+}$ could also be deprotonated easily in water, with pK_a values of 7.6 ± 0.3 (Figure 5) and 5.7 ± 0.3, respectively. Overall, the pKa values of this family of complexes were found to be around 7, suggesting that variations in the ligand structures could lead to different protonation states present under biologically neutral pH conditions.

2.2.4 pUC19 Agarose gel electrophoresis

Metal complexes show a wide range of interactions with DNA, from coordination bonding to DNA cleavage, intercalation, or groove binding.[42] One method to investigate and distinguish the different kinds of DNA-metal complex interactions is by agarose gel electrophoresis using plasmids. The native plasmid pUC19 is circular and consists of two topological forms, i.e., a supercoiled (SC) form which migrates fastest as it has a compact structure, and a slower-migrating, less compact, open circular form (OC). If addition of the potential DNA binder results in single-stranded breaks in DNA, the SC band will disappear while the OC band signal increases in a concentration-dependent manner. When the potential DNA binder causes double-stranded breaks in DNA, the SC form will again disappear to form a new band corresponding to the linear product, which runs at a position between the SC and the OC bands.[43] Here, agarose gels (Figure

6) were loaded as follows: lane 1 and 10 contained the reference gene ruler molecular ladders, lane 2-9 all consisted of a constant DNA base pairs concentration of $5 \bullet 10^{-11}$ M where lane 2 was the pure DNA control and lane 3-9 contained increasing ratios of metal complex (MC) to base pair (BP) concentration. The gels were stained with SyBr safe after electrophoresis to eliminate potential interactions of the stain with DNA. As the metal complexes can easily be deprotonated in solution, the interactions with the plasmid were studied by incubating the complex and DNA prior to performing the gel electrophoresis at two different pH values, namely 4.5 and 8.0.

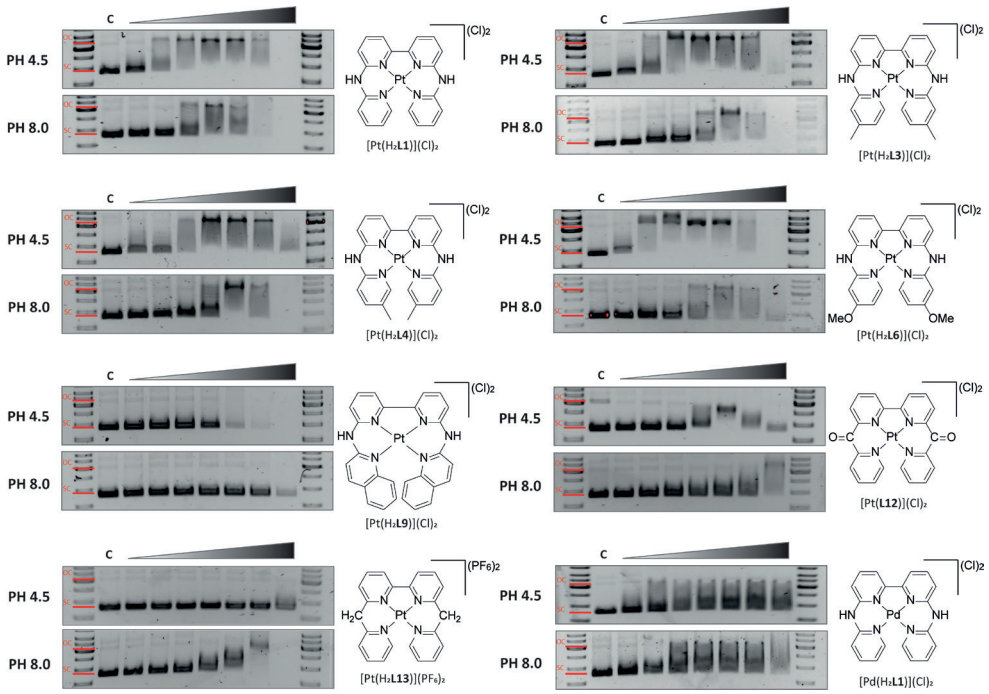

Figure 6. Agarose gel electrophoresis analysis of the interactions of pUC19 plasmid DNA and d^8 metal tetra-pyridyl complexes at pH 4.5 and 8. Lane 1 and 10 contain the molecular ladders, lane 2 is the pUC19 DNA plasmid only control and lane 3-9 contained increasing metal complex (MC) to base pair (BP) concentration ratios (0.05, 0.1, 0.2, 0.5, 1, 2, 5).

The gel of $[Pt(H_2\mathbf{L1})]^{2+}$ (Figure 6) at pH 4.5 showed not only concentration-dependent migration retardation, but also diminished signal with increasing metal complex concentration. DNA cleavage, however, was not observed, and coordination interactions are unlikely with such complexes as they have a saturated coordination sphere. Therefore, the interaction visualized on these gels is most probably intercalation or groove binding, as both types of interaction unwind DNA and alter the SC topology to the OC. The diminished fluorescence signal was attributed to saturation of the DNA by the metal complex, which left fewer binding sites available for the binding of the DNA-

imaging agent SyBr safe. Interestingly, the gel of $[Pt(H_2\mathbf{L1})]^2$ at pH 8.0 showed similar results but required a higher concentration of metal complex than the gel at pH 4.5, as the minimal metal complex to base pair ratio required to visualize interactions was 0.2 *vs*. 0.05, respectively. Whether this effect was caused by the protonation of the metal complex at pH = 4.5, or whether a more acidic pH facilitates the topology change of DNA at lower concentration, is unclear. Similar behavior was seen for platinum complexes $[Pt(H_2\mathbf{L3})]^{2+}$, $[Pt(H_2\mathbf{L4})]^{2+}$, and $[Pt(H_2\mathbf{L6})]^{2+}$ (Figure 6), while complexes $[Pt(H_2\mathbf{L2})]^{2+}$ $[Pt(H_2\mathbf{L5})]^{2+}$, $[Pt(H_2\mathbf{L7})]^{2+}$, and $[Pt(H_2\mathbf{L8})]^{2+}$ (Figure SI.21), showed no clear interactions apart from smudging of the DNA signal. However, the lack of interactions visualized on the gel does not necessarily indicate chemical inertness of these compounds. Intercalation and groove binding interactions are frequently undetectable using plasmid agarose electrophoresis as, in particular, positively charged metal complexes may dissociate during electrophoresis. This effect may result in false negatives, where only the native SC and OC bands can be visualized.[44] The difference observed here between the different platinum compounds might, therefore, not accurately reflect their different interaction with DNA, but it did provide insight into the retention capability of the DNA-metal complex association during electrophoresis. Interestingly, compound $[Pt(H_2\mathbf{L9})]^{2+}$ only showed pH-dependent intensity of the emissive bands, but no changes of the electrophoretic properties of DNA. This observation implies that the interactions between the metal complex and DNA impeded the binding of SyBr safe, but without unwinding or causing topology changes of the DNA. Complexes $[Pt(\mathbf{L10})]^{2+}$ and $[Pt(\mathbf{11})]^{2+}$ do not have an acidic proton and should, therefore, not be affected by pH changes. Indeed, neither compounds showed any change in migration nor a decreasing intensity when the pH was varied. $[Pt(\mathbf{L12})]^{2+}$ showed, upon increasing the metal complex concentration, first a gradual decrease of the DNA electrophoretic mobility, followed by an increase of the electrophoretic mobilities at pH 4.5. We interpret this observation as the result of unwinding of the negatively supercoiled form, first to an open circular form, and in a second stage to the positively supercoiled form. This behavior is demonstrative of intercalation[45] and it was not duplicated at pH 8. It insinuated a key role of hydrogen bonding in the interaction between the metal complex bearing a bridging carbonyl group and DNA. $[Pt(H_2\mathbf{L13})]^{2+}$ subverted expectations as the only metal complex that showed strong interaction at pH 8.0 but minimal interactions at pH 4.5, indicating that the deprotonated methylene group and electrostatic interactions are pivotal in the interactions between DNA and compound $[Pt(H\mathbf{L13})]^{1+}$.

In most cases, the palladium complexes (figures SI.21, SI.22) interacted in a very similar fashion compared with their platinum analogues, suggesting that the key defining parameter for the interaction of these metal complexes with DNA is the functional groups on the ligand rather than the difference in the metal center. On the other hand, three palladium complexes, i.e., $[Pd(H_2\mathbf{L1})]^{2+}$, $[Pd(H_2\mathbf{L7})]^{2+}$ and $[Pd(\mathbf{L10})]^{2+}$, did show

distinctive behavior, compared with their platinum analogues. [Pd(H_2**L1**)]$^{2+}$ did show changes in migration and increased interactions at acidic pH, but to a lesser extent than its platinum analogue. Both [Pd(H_2**L7**)]$^{2+}$ and [Pd(**L10**)]$^{2+}$ showed gradual unwinding from the negative SC band to the OC band and finally to the positively charged SC band at pH 4.5, as mentioned above, which is characteristic of intercalation. Such observations were neither made at pH 8 nor for their platinum analogues.

2.2.5 Calf thymus DNA titrations

The interactions between the metal complexes and dsDNA was further studied by UV-vis spectroscopy in titration experiments. Varying amounts of calf thymus DNA (3-666 µM base pairs) were added to a solution of the metal complex at a fixed concentration (33 µM) in a 96-well plate at a pH of 5.0 or 8.0. The absorbance in each well was then measured with a plate reader, which afforded a convenient and fast method to screen the interactions at different pH.

At pH 5, almost all compounds showed a decrease in absorbance and a red shift of the absorption maximum around 400 nm upon increasing DNA concentration. The clear isosbestic points suggested the presence of only two interconverting absorbing species, as seen for [Pt(H_2**L3**)]$(Cl)_2$ and Pt[(H_2**L7**)]$(Cl)_2$ in Figure 7 (all other measurements are reported Appendix I figures SI.23-SI.46). The species present in solution in absence of DNA is the unbound, bis-protonated metal complex, while the second species is an adduct between the metal complex and DNA. The hypochromism and bathochromic shift are strong indicators of intercalation of the metal complexes in the DNA helix.[46] The spectra of the four complexes [Pt(H_2**L9**)]$(Cl)_2$, [Pt(**L12**)]$(Cl)_2$, [Pd(H_2**L9**)]$(Cl)_2$, and [Pd(H_2**L13**)]$(Cl)_2$ showed no clear difference whether high concentrations of DNA were used or not, indicating that these metal complexes were either inert, or that their interaction with DNA led to minimal spectroscopic changes. The lack of changes for complexes [Pt(H_2**L9**)]$(Cl)_2$ and [Pd(H_2**L9**)]$(Cl)_2$ is especially noteworthy and might be explained by the increased helical distortion and overall bulkiness reducing the planarity of the complex, which is a key property required for intercalation.[47]

At pH 8, titrations of [Pt(**L10**)]$(Cl)_2$, [Pt(**L11**)]$(Cl)_2$, and [Pd(**L10**)]$(Cl)_2$ showed identical spectra, compared to those obtained at pH 5. Such similar behavior can be interpreted as a consequence of the absence of an acidic NH bridge for these compounds. Compound [Pd(H_2**L5**)]$(Cl)_2$ also showed no difference between pH 5 and pH 8, which can be attributed to the high pK_a for [Pd(H_2**L5**)]$(Cl)_2$, resulting in the compound being fully protonated even at a pH of 8. All other metal complexes in this series showed similar behavior, characterized by i) a considerable dependence of the UV-vis spectrum of the mixture on DNA concentration, ii) a lack of isosbestic points, suggesting the presence of at least 2 reactions and 3 interconverting species upon increasing the pH in presence of DNA. For example, protonation might be *followed by* intercalation, when titration

was performed at a pH at which the initially DNA-free complex is in its deprotonated form. Interestingly, each metal compound showed almost identical spectra at high DNA concentration (666 µm) for both pH values, indicating that both titrations led to the same DNA-bound species.

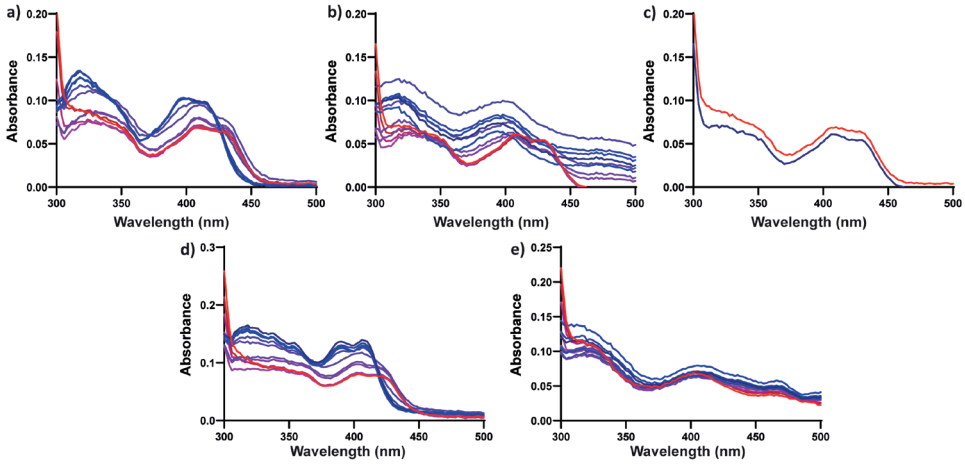

Figure 7. Absorbance spectra of calf thymus DNA titrated with metal complexes. The blue to red color gradient represents increasing DNA concentrations ranging from 0 to 666 µM base pairs, respectively. a) $[Pt(H_2\mathbf{L3})](Cl)_2$ at pH 5. b) $[Pt(H_2\mathbf{L3})](Cl)_2$ at pH 8. c) Spectra in presence of 666 µM DNA for $[Pt(H_2\mathbf{L3})](Cl)_2$ at pH 5 (red) and 8 (blue). d) $[Pt(H_2\mathbf{L7})](Cl)_2$ at pH 5. e) $[Pt(H_2\mathbf{L7})](Cl)_2$ at pH 8

The data showed that fully protonated metal complexes lack absorbance above 450 nm, while absorbance above 450 nm indicates at least partial deprotonation. The titration spectra at high DNA concentration did not display any absorbance above 450 nm, leading to the conclusion that the metal complex, when fully bound to DNA, is also fully protonated. The compounds $[Pt(H_2\mathbf{L7})](Cl)_2$, $[Pt(H_2\mathbf{L8})](Cl)_2$, and $[Pd(H_2\mathbf{L8})](Cl)_2$, however, showed no interactions for the titration at pH 8 and share a strikingly low pK_a of 6.3 ± 0.1 and lower. The low pK_a indicates that the free metal compounds exist only in the once-deprotonated state at pH 8 and in both protonation states at pH 5, which suggests, in turn, a pivotal role of pH for the binding of this family of complexes to DNA. Overall, it appears these metal complexes need to be doubly protonated to be able to interact with DNA and form a DNA adduct. Notably, the reduction of the overall charge of the complex from +2 to +1 upon deprotonation, may hinder the stabilization of the intercalated adduct due to lowered attraction with the negatively charged phosphate groups of DNA.

2.2.6 Binding constant

Though fast and convenient, the measurements described in section 3.5 used 96-well plates and a Tecan reader, which is associated with small volumes and low optical pathways. These conditions led to lower resolution and increased noise, compared with high-end UV-vis spectrometers measuring the absorbance of 3 mL samples over 1 cm optical path length, which prevented the accurate calculation of binding constants to DNA. Binding constants were determined by UV-vis absorption titrations of solutions of a higher volume on a high-end spectrometer, with a constant metal complex concentration (100 µM) and varying amounts of calf thymus DNA (100-400 µM base pairs). Here the pH was kept constant and acidic (4.5) to ensure full protonation of the metal complexes, which appears to be required for strong binding. Furthermore, discrepancies attributed to aggregation were observed at low DNA concentrations. Therefore, only the titration points where [M] ≤ [DNA] were used to determine the binding constant. The fraction of bound metal complex (α) was calculated by Equation **1** where and are the absorbance of the DNA-free and fully bound metal complex, respectively, A is the measured absorbance at each DNA concentration. Equations (2) and (3) were used to calculate the and values necessary to plot a Scatchard plot, as seen for [Pt(H$_2$**L1**)](Cl)$_2$ and [Pt(H$_2$**L13**)](PF$_6$)$_2$ in Figure 8, where and are the concentration of the metal complex and the DNA base pair concentration, respectively. is the concentration of the free metal complex when the equilibrium is reached, is the amount bound metal complex per BP of DNA. All other Scatchard plots can be found in the Appendix I figures SI.47-SI.57.

$$\alpha = \frac{(A_f{}^0 - A)}{(A_f{}^0 - A_b{}^0)} \qquad \text{Equation (1)}$$

$$r = \alpha \frac{M}{DNA} \qquad \text{Equation (2)}$$

$$M_f = (1 - a)M \qquad \text{Equation (3)}$$

$$\frac{r}{M_f} = K(1 - nr)\left[\frac{1-nr}{1-(n-1)r}\right]^{n-1} \qquad \text{Equation (4)}$$

The Scatchard plots were then fitted to the McGhee-von Hippel model in Equation (4),[48] which has been extensively used to determine binding constant and the binding site size in base pairs for intercalators.[49,50] The determined experimental values are recorded in Table 5. Ethidium bromide was measured as a control and the value found (K = 1.9•10^5 M^{-1}) was in accordance with literature values.[50] According to our data, the binding constant for most complexes was around 10^5 M^{-1}. The nature of the metal (palladium or platinum) did not have any significant effect on the binding constant. Likewise, small modification of the terminal pyridine of these H$_2$bapbpy-based ligands

led to minimal changes in the values of K. Modifications of the bridging NH groups, however, did show significant effects: in the case of the compound with methylated NMe bridges, [Pt(**L10**)]$(PF_6)_2$, the binding constant decreased to $1.6 \bullet 10^4$ M^{-1}. Similarly, the compound [Pt(H_2**L13**)]$(Cl)_2$ which features methylene bridges, also showed a reduced binding constant of $5.3 \bullet 10^4$ M^{-1}. These results highlight the pivotal role of the protonated bridging NH groups, and hence of hydrogen bonding, for the strength of the interactions between these metal complexes and calf thymus DNA. On the other hand, [Pt(**L11**)]$(PF_6)_2$, which contained bridging thioether groups, appears to be an exception in this series, with a high binding constant of $1.5 \bullet 10^5$ M^{-1} while the thioether groups cannot be deprotonated. It should be noted that the charge of all these compounds was identical (2+), which illustrates that the decrease (or increase) in binding constant is not related to changes of the electrostatic interaction by reduction of the charge, but must involve a combination of H-bonding properties, hydrophobicity, and/or dipole moments. Compounds that were incapable of deprotonation were also titrated at pH 8 to determine the influence of pH on DNA binding. Ethidium bromide ($K = 2.4 \pm 0.2 \bullet 10^5$ $M,^{-1}$ $n = 1.9 \pm 0.1$), [Pt(H_2**L10**)]$(PF_6)_2$ ($K = 1.0 \pm 0.2 \bullet 10^4$ $M,^{-1}$ $n = 2.6 \pm 0.4$), and [Pt(H_2**L11**)] $(PF_6)_2$ ($K = 1.0 \pm 0.1 \bullet 10^5$ $M,^{-1}$ $n = 2.3 \pm 01$) showed similar binding constants at pH 8.0 and 4.5, underlining that pH had a minimal effect on the metal complex-DNA interaction itself in absence of a protonation/deprotonation event, and that the different titration curves observed at pH 4.5 and pH 8 for compounds with a proton-labile group, are a direct result of the varying propensity of the metal complexes to be re-protonated when DNA is added.

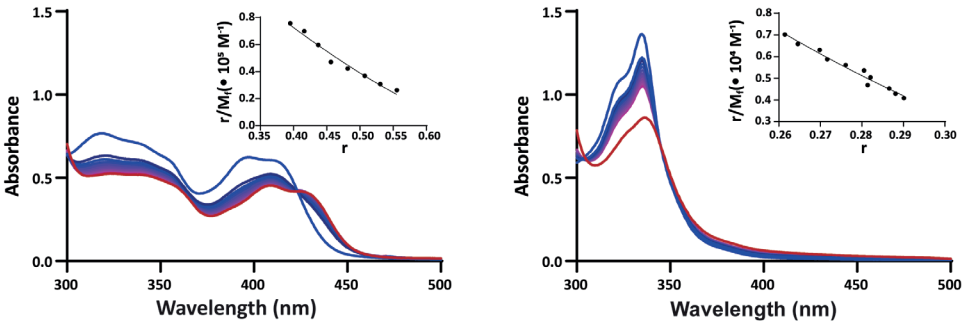

Figure 8. Evolution of the UV-vis spectrum of a 100 µM solution of [Pt(H_2**L1**)]$(Cl)_2$ (left) and [Pt(H_2**L13**)]$(PF_6)_2$ (right) titrated with calf thymus DNA at pH 4.5. The blue to red gradient represents increasing DNA concentration from 0 to 360 µM base pairs, respectively. The inlays are Scatchard plots (dots) fitted to the McGhee–von Hippel model (plain line).

Table 4. Binding constants (K) and binding size (n) for the calf thymus DNA titration of different $[M(H_2L)]^{2+}$ complexes at a pH of 4.5, fitted to the McGhee–von Hippel model.

		M = Pt^{II}		M = Pd^{II}	
Ligand	R	K (10^5 M^{-1})	n	K (10^5 M^{-1})	n
H_2**L1**		2.4 ± 0.4	1.5 ± 0.1	2.6 ± 0.5	1.9 ± 0.1
H_2**L2**	3-Me	1.7 ± 0.3	1.7 ± 0.1	2.0 ± 0.3	2.0 ± 0.1
H_2**L3**	4-Me	2.9 ± 0.7	1.3 ± 0.1	5 ± 1	2.1 ± 0.1
H_2**L4**	5-Me	1.2 ± 0.2	1.7 ± 0.1	3.3 ± 0.9	2.0 ± 0.1
H_2**L5**	6-Me	1.4 ± 0.3	1.9 ± 0.1	1.7 ± 0.3	2.1 ± 0.1
H_2**L6**	4-OMe	3.7 ± 0.9	2.1 ± 0.1	4 ± 1	2.1 ± 0.1
H_2**L7**	4-Cl	1.0 ± 0.3	1.7 ± 0.1	-[1]	-[1]
H_2**L8**	4-CF_3	-[1]	-[1]	-[1]	-[1]
H_2**L9**		-[1]	-[1]	-[1]	-[1]
L10		0.16 ± 0.05	2.9 ± 0.5	-[1]	-[1]
L11		1.5 ± 0.2	2.3 ± 0.1	n.d.	n.d.
L12		n.d.	n.d.	n.d.	n.d.
H_2**L13**		0.53 ± 0.02	2.6 ± 0.1	-[1]	-[1]

[1] Binding constant could not be determined due to aggregation of the metal complex. n.d. = not determined.

2.3 Discussion

The structure-activity relationship for the interaction of $[M(H_2bapbpy)]^{2+}$ metal complexes and DNA highlighted several trends. First, small functional group addition to the H_2bapbpy ligand did not necessarily result in significantly different interaction of the corresponding metal complexes with DNA. Compounds $[M(H_2$**L1-L8**$)]^{2+}$ showed similar behavior at low pH, where all metal complexes are in the bicationic state. The plate reader and the high-end UV-vis analysis of the DNA titrations afforded similar binding constants of ~10^5 M^{-1} at low pH. Even though these binding constants were found similar, the results of the DNA agarose gel electrophoresis analysis varied strongly between these different complexes, indicating that the ability of the metal complex-DNA adduct to "survive" the conditions of gel electrophoresis does not correlate directly with the binding strength, and thus seems incidental. Complexes $[M(H_2$**L9**$)]^{2+}$ appear as aberrations in the series: they showed interactions that were probably not intercalation, likely because of the reduction of planarity imposed by the sterically hindered ligand. The complexes where the bridging amine group was modified exhibited more variations: the binding constant for the thioether platinum complex $[Pt($**L11**$)]^{2+}$ was found to be ~10^5 M^{-1}, whereas the methylated bridging nitrogen compound $[Pt($**L10**$)]^{2+}$ and the bridging methylene compound $[Pt(H_2$**L13**$)]^{2+}$ showed lower binding constants of ~10^4 M^{-1}.

An interesting change in behavior was observed at higher pH as the DNA titration experiments showed two steps namely, protonation and intercalation, while the metal complexes with pK_a lower than 6.3 ± 0.1 showed no interactions at all at a pH 8. These observations indicate that the fully protonated bicationic state is required for intercalation to occur, which is, at least partly present at pH 8 for the complexes with a

pK_a above 6.3. This partial presence facilitates intercalation and allows the equilibrium to be shifted towards complete intercalation and protonation of the metal complexes at high DNA concentration (666 µM). The requirement of a certain level of protonation for intercalation to occur is interesting, although stronger DNA intercalation is often reported for protonated compounds at low pH.[51] Hammarson *et al.* reported spiropyran photoswitches that bonded 35 to 66 times stronger in their protonated forms in comparison to the deprotonated analogues. Jana *et al.* reported a naphthalene diimide analogue that showed not only significantly stronger binding at pH 5 than pH 7, but also a change in binding mechanism.[52] The compound showed threading intercalation at pH 5 while the main mechanism was minor groove binding at pH 7. Therefore, the pivotal significance of the pKa and protonation state, as elucidated in this study aligns seamlessly with existing literature.

2.4 Conclusion

In this work we describe the synthesis of 24 metal complexes based on the $[Pt(H_2bapbpy)]^{2+}$ scaffold, 23 of which were characterized crystallographically. Generally, the structures of these metal complexes in the solid state are similar, and the small modification of the H_2bapbpy scaffold did not result in important structural changes. The position of the methyl substituents and of the electron-donating groups on the terminal pyridines had minimal influence on the pK_a of the complexes, while the presence of the electron-withdrawing CF_3 groups resulted in a decrease by 2 pK_a units. Calf thymus DNA titration showed hypochromism (a decrease in absorbance), and a bathochromic shift for the absorbance of the metal complex with increasing DNA concentration, strong indicators that most metal complexes interact with DNA by intercalation. The binding constants were determined to be around 10^5 for most compounds and only decreased to 10^4 when the bridging nitrogen was methylated or replaced by a bridging methylene, orders of magnitude commonly associated with intercalation. The DNA titrations at pH 8 and 5 showed that protonation of both bridges is crucial for intercalation to occur, as the bridging nitrogen of the formed DNA-metal complex abduct is fully protonated at both pHs, resulting in identical absorbance spectra. However, low pK_a compounds that were fully monodeprotonated at pH 5 showed no interactions with DNA at all. This leads to the conclusion that the differences in behavior at pH 4.5 and 8 result directly from the protonation state of the metal complex, which is critical in the interactions between DNA and metal complex.

2.5 Experimental

2.5.1 UV-VIS pK_a determination

pK_a values were determined according to a literature procedure.[41] Stock solution of the compounds were prepared by dissolving 1-2 mg in DMSO (200 µl) and adjusted with water for a final concentration of 10 mM. A control stock solution was made by DMSO (200 µl) in H_2O (800 µl). The buffer solutions in the pH range 2.5-12.0 were prepared in 0.5 increments. Buffer composition for pH range 2.5-3 was Citric acid/citrate, for pH 3.5-5.5 acetic acid/sodium acetate, for pH 6-8 KH_2PO_4/K_2HPO_4, and pH 8.5-12 was $Na2HPO_4/Na_3PO_4$. The solutions were adjusted with 0.1 M KCl solution to maintain a constant ionic strength of 0.1 M. The range of buffer solution (190 µL) and stock or control solution (10 µL) were added to a 96-wells microplate and the absorbance of each well was measured between 300 and 600 nm by a M1000 Tecan reader. Three wavelengths were chosen per titration that showed maximal variation in absorbance. Two separate experiments were then used to calculate 95% confidence interval of the pK_a.[53]

2.5.2 PUC19 DNA interactions on agarose gel

Binding interactions of the metal complexes and pUC19 DNA plasmid were studied with 0.9 % agarose TAE gels. The DNA stock solution was prepared by a 6 times dilution of the commercially available pUC19 plasmid (1mg/ml). The metal complexes were dissolved in a phosphate (NaH_2PO_4) buffer (100 mM), unadjusted for pH 4.5 and adjusted with aqueous NaOH solution (10 M) to pH 8.0. The DNA stock (2 µl, $5 \bullet 10^{-10}$ mol basepairs) was incubated for 15 minutes with varying amounts of metal complex (MC) to achieve BP/MC ratios of 0.05, 0.1, 0.2, 0.5, 1, 2, 5 and no metal complex to form the DNA control. The total volume was adjusted to 20 µL by addition of the corresponding phosphate buffer. After incubation, Loading dye (4 µl 6X) was added to the samples and 10 µL was loaded in lanes 2-9. The DNA control ladder was prepared by GeneRuler DNA ladder (2 µL), loading dye (2 µL, 6x) and phosphate buffer (8 µL) and was loaded (4 µL) into lanes 1 and 10. The gel was run at 80 V for 90 minutes in TAE running buffer. After electrophoresis, the gels were stained for 20 minutes in a SYBR safe staining solution (10 µL in 200 mL H_2O). Afterwards, the gels were destained for 15 minutes in H_2O and directly imaged.

2.5.3 Calf thymus titration at pH 5 and 8

Titrations of the metal complexes by calf thymus DNA were performed at pH 5 and pH 8. The calf thymus DNA basepair concentration was determined from absorbances at 260 nm using ε_{260} =12,824 and further diluted in water.[54] The metal complex stock solutions were prepared by dissolving 1-2 mg in the corresponding volume of DMSO to form a 10 mM solution, which was subsequently diluted with water to form stock

solutions (100 μM). The two buffer solutions were prepared as 100 mM solution of AcONa for 5 pH and 100 mM NaH_2PO_4 for pH 8. To each well of a 96-wells microplate was added metal complex stock (50 μL), Buffer pH 5 or 8 (50 μL), calf thymus DNA (0-50 μL) and water for a final volume of 150 μL and was incubated for 15 min before analysis by a M1000 Tecan reader.

2.5.4 Binding constant determination by calf thymus titration

Binding constants were measured by titration of a metal complex solution with calf thymus DNA. Metal complex solution (100 μM) in pH 4.5 buffer (100 mM, NaH_2PO_4) were prepared and titrated with an aqueous calf thymus DNA solution (6 mM). The first DNA aliquot had a volume of 50 μl followed by 10 aliquots of 7 uL and a final large aliquot of 50 ul to achieve full saturation. After the addition of each aliquot the solution was incubated for 3 minutes to reach equilibrium, before measuring the absorbance from 300 nm to 500 nm on a Cary 60 UV-Vis Spectrophotometer by Agilent. The required incubation time was determined in optimization experiments prior to the main titration.

2.5.5 Synthesis

All commercially available reagents were ordered from Sigma-Aldrich and were used as received.

N-methoxy-*N*-methylpicolinamide,[55] 6,6'-diamino-2,2'-bipyridine,[28] ligands H_2**L2**-**5**, H_2**L9**[27] and metal complexes $[M(H_2\mathbf{L1})](Cl)_2$[26] were prepared according to literature procedures. Filters used were Whatman® regenerated cellulose membrane filters, RC60 Membrane Circles, diam. 47 mm, pore size 1 μm. NMR spectra were recorded on a Bruker, AV-300, AV-400, AV-500, AV-600, or AV-850 spectrometers. High resolution mass spectra (HRMS) were recorded on Waters XEVO-G2 XSQ-TOF) mass spectrometer equipped with an electrospray ion source in positive mode (source voltage 3.0 kV, desolvation gas flow 900 L/hr, temperature 250 °C) with resolution R= 22000 (mass range m/z = 50-2000) and 200 pg/uL Leu-enkephalin (m/z = 556.2771) as a "lock mass".

2.5.5.1 6,6'-dibromo-2,2'-bipyridine

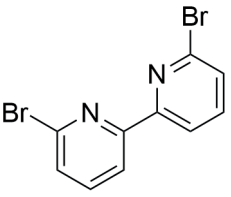

A suspension of 6,6-dibromopyridine (30.0 g, 127 mmol) in diethyl ether (278 mL) under nitrogen atmosphere was cooled to −95 °C. A solution of n-BuLi in 2.5 M hexane (55.7 mL, 139 mmol) was slowly added dropwise over the course of half an hour. The reaction mixture turned yellow and was stirred for an additional hour, after which copper(II) dichloride (7.78 g, 58 mmol) was added and the reaction was stirred for another hour. Oxygen gas was then bubbled through the reaction mixture for 1 h, resulting in a brown suspension.

The reaction mixture was allowed to warm to room temperature and 6 M HCl (100 mL) was added. The mixture was filtered, and the residue was resuspended in methanol, briefly sonicated for 5 min, filtered and dried overnight to afford the title compound as a white solid. Yield 12.1 g, 39 mmol, 61%. **^{1}H NMR** (400 MHz, Chloroform-d) δ 8.38 (d, *j* = 7.7 Hz, 2H), 7.67 (t, *j* = 7.8 Hz, 2H), 7.51 (d, *j* = 7.8 Hz, 2H). **^{13}C-NMR** (101 MHz, Chloroform-d) δ 155.6 (Cq), 141.6 (Cq), 139.3 (CH), 128.6 (CH), 120.2 (CH).

2.5.5.2 H_2L1

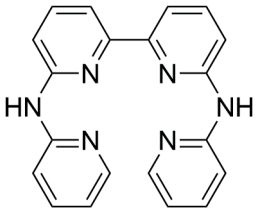

6,6'-Dibromo-2,2'-bipyridine (1.25 g, 4.00 mmol), Pd(dba)2 (150 mg, 0.26 mmol), (Rac)-BINAP (311 mg, 0.50 mmol) and potassium *t*-butoxide (3.62 g, 32.2 mmol) were dissolved in toluene (150 mL). Afterwards, 2-aminopyridine (827 mg, 8.8 mmol) was added and the reaction was refluxed for 3 days. The suspension was allowed to cool to room temperature and water (200 mL) was added. The mixture was stirred vigorously for 1 h and was either filtered if a suspension was formed, or in lack thereof (2); The layers were separated, the organic layer was dried with magnesium sulfate, filtered and concentrated in vacuo, to afford ligand H_2**L1**. Yield 1.01 g, 2.9 mmol, 74%. if necessary, the crudes were further purified by precipitation by $CHCL_3$/diethylether. **^{1}H NMR** (500 MHz, DMSO-d6) δ 9.75 (s, 2H), 8.25 (d, *j* = 3.1 Hz, 2H), 7.97 (d, *j* = 8.4 Hz, 2H), 7.85 (d, *j* = 6.4 Hz, 2H), 7.82 (t, *j* = 7.7 Hz, 2H), 7.75 – 7.71 (m, 2H), 7.67 (d, *j* = 7.0 Hz, 2H), 6.92 – 6.88 (m, 2H). **^{13}C NMR** (126 MHz, DMSO-d6) δ 154.9 (Cq), 154.4 (Cq), 154.1 (Cq), 148.1 (CH), 139.0 (CH), 138.2 (CH), 116.6 (CH), 113.0 (CH), 112.7 (CH), 112.2 (CH).

2.5.5.3 H_2L6

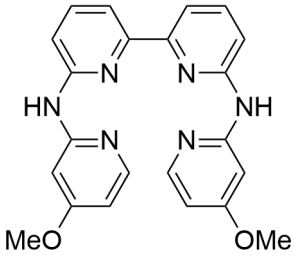

Compound H_2**L6** was synthesized according the procedure for H_2**L1**. Starting 6,6'-Dibromo-2,2'-bipyridine (4 mmol scale), but with 2-Amino-4-Methoxypyridine instead of 2-aminopyridine to afford ligand H_2**L6**. Yield 784 mg, 2.0 mmol, 49%. **Rf** 0.9 (95/5 DCM/MeOH). **^{1}H NMR** (500 MHz, DMSO-d6) δ 9.75 (s, 2H), 8.07 (d, *j* = 5.8 Hz, 2H), 7.84 – 7.76 (m, 6H), 7.55 (d, *j* = 6.9 Hz, 2H), 6.54 (dd, *j* = 5.8, 2.4 Hz, 2H), 3.87 (s, 6H,). **^{13}C NMR** (126 MHz, DMSO-d6) δ 166.95 (Cq), 156.40 (Cq), 154.62 (Cq), 154.04 (Cq), 149.16 (CH), 138.86 (CH), 112.89 (CH), 112.72 (CH), 104.80 (CH), 96.38 (CH), 55.61 (CH_3).**HR-MS** $[M+H]^+$: 401.17205 (calculated) 401.17135 (measured).

2.5.5.4 H_2L7

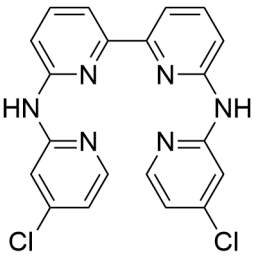

Compound H_2**L7** was synthesized according the procedure for H_2**L1**. Starting 6,6'-Dibromo-2,2'-bipyridine (4 mmol scale), but with 2-Amino-4-chloropyridine instead of 2-aminopyridine to afford ligand H_2**L7**. Yield 1.1 gram, 2.7 mmol, 67%. The compounds proved insoluble in common solvents, such as DMSO and $CDCl_3$, preventing full NMR characterization and HRMS. The ligand was used in subsequent reactions without futher characterization and regarded pure for molar equivalent calculations.

2.5.5.5 H_2L8

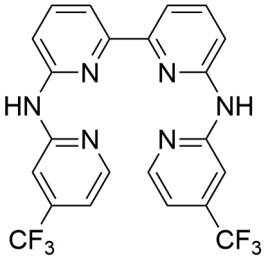

2,2'-bipyridine-6,6'-diamine (200 mg, 1.07 mmol, 1.00 eq), $[Pd(dba)_2]$ (12 mg, 0.02 mmol), (rac)BINAP (40 mg, 0.06 mmol), potassium *t*-butoxide (520 mg, 4.6 mmol) were dissolved in toluene (20 mL). Afterwards 2-bromo-4-(trifluoromethyl) pyridine (610 mg, 2.7 mmol) was added and the reaction was refluxed for 3 days. The suspension was allowed to cool to room temperature and water (200 mL) was added. The mixture was stirred vigorously for 1 h and was filtered dried in vacuo overnight, to afford ligand H_2**L8**. Yield 380 mg, 1.07 mmol, 75%. **Rf** 0.7 (95/5 DCM/MeOH). **^{1}H NMR** (600 MHz, DMSO-d6) δ 10.34 (s, 2H), 8.65 (s, 1H), 8.52 (d, *j* = 5.2 Hz, 2H), 7.91 – 7.83 (m, 4H), 7.53 (dd, *j* = 7.6, 1.5 Hz, 2H), 7.24 (dd, *j* = 5.3, 1.6 Hz, 2H). **^{13}C NMR** (151 MHz, DMSO-d6) δ 154.83 (Cq), 153.51 (Cq), 153.26 (Cq), 138.76 (CH), 137.83 (CH), 112.80 (CH, CH), 110.98 (CH), 107.03 (CH). **^{19}F NMR** (471 MHz, DMSO-d6 + TFA-d) δ -65.54 (CF_3). **HR-MS** $[M+H]^+$: 477.12569 (calculated) 477.12533 (measured).

2.5.5.6 L10

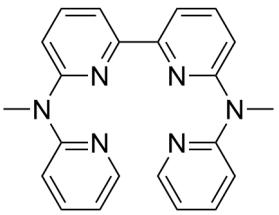

H_2**L1** (98 mg, 0.29 mmol) and KOH (132 mg, 2.4 mmol) were dissolved in dry DMF (1.8 mL) and the reaction was stirred at room temperature for 1 h under nitrogen atmosphere. MeI (0.07 mL, 1 mmol) was added and the flask was covered with aluminum foil and left overnight. The reaction was quenched with water (60 mL). The aqueous layer was extracted with EtOAc (3x 70 mL) and the organic layers were combined and washed with water (75 mL) and brine (75 mL). The organic layer was dried with magnesium sulfate, filtered and the solvents were removed in vacuo. The crude was further purified by silica column (DCM > 98/2 DCM/MeOH). Ligand **L10** was obtained as a yellow solid. Yield 70 mg, 0.19 mmol, 66%. **^{1}H NMR** (500 MHz, Chloroform-d) δ 8.38

(d, *j* = 3.8 Hz, 2H), 7.97 (d, *j* = 7.5 Hz, 2H), 7.65 (t, *j* = 4.0 Hz, 2H), 7.56 (ddd, *j* = 9.0, 7.2, 2.0 Hz, 2H), 7.30 (d, *j* = 8.4 Hz, 2H), 7.19 (d, *j* = 8.2 Hz, 2H), 6.88 (dd, *j* = 6.4, 5.0 Hz, 2H), 3.74 (s, 6H). **^{13}C NMR** (126 MHz, Chloroform-d) δ 157.9 (Cq), 156.9 (Cq), 154.6 (Cq), 148.1 (CH), 138.1 (CH), 137.1 (CH), 116.9 (CH), 114.7 (CH), 114.1 (CH), 114.0 (CH), 36.1 (14). **HR-MS** $[M+H]^+$: 369.18190 (calculated) 369.18190 (measured).

2.5.5.7 L11

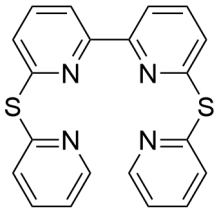

2-Mercaptopyridine (354 mg, 3.18 mmol), 6,6'-dibromo-2,2'-bipyridine (500 mg, 1.59 mmol) and potassium carbonate (1.50 g, 10.9 mmol) were dissolved in dimethylformamide (20 mL) and refluxed overnight. The reaction mixture was allowed to cool to room temperature and water (20 mL) was added. The precipitate was filtered and dried under vacuum overnight. The crude was then dissolved in $CHCL_3$ (20 mL) and reprecipitated by the addition of diethyl ether (50 mL). The suspension was filtered and dried in vacuo to afford ligand **L11** as a white solid. Yield 267 mg, 0.78 mmol, 45%. **Rf** 0.9 (98/2 DCM/MeOH). **^{1}H NMR** (400 MHz, DMSO-d6) δ 8.56 (ddd, *j* = 4.8, 2.0, 0.9 Hz, 2H), 8.00 (d, *j* = 6.9 Hz, 2H), 7.89 (t, *j* = 7.8 Hz, 2H), 7.83 (td, *j* = 7.7, 2.0 Hz, 2H), 7.59 (d, *j* = 8.0 Hz, 2H), 7.50 (d, *j* = 6.9 Hz, 2H), 7.36 (ddd, *j* = 7.4, 4.8, 1.1 Hz, 2H). **^{13}C NMR** (101 MHz, DMSO-d6) δ 156.06 (Cq), 155.38 (Cq), 154.87 (Cq), 150.26 (CH), 138.84 (CH), 137.78 (CH), 126.28 (CH), 125.71 (CH), 122.54 (CH), 118.58 (CH). **HR-MS** $[M+H]^+$: 375.07326 (calculated) 375.07252 (measured).

2.5.5.8 L12

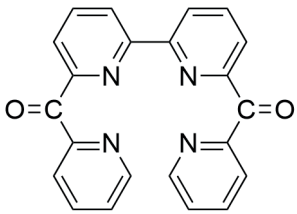

n-Butyllithium (12.5 ml of 1.6 M, 20 mmol) in dry THF (100 ml) under nitrogen atmosphere was cooled to −95 °C by a liquid nitrogen and aceton bath. A solution of 6,6'-dibromo-2,2'-bipyridine (3.14 g 10 mmol) in dry THF (150 mL) was then slowly dropped into the cooled solution and the solution became dark red over 1 h. *N*-methoxy-*N*-methylpicolinamide (3.9 g, 24 mmol) in dry THF (30 mL) was added dropwise. After addition the reaction was again cooled to −95 °C and then slowly allowed to warm up to room temperature overnight. The reaction mixture was quenched with aqueous 1 M HCl (200 mL) and extracted with DCM (100) mL. NaOH pellets were ground up and added to the water layer until the pH of the solution became 10 and a precipitate formed. The precipitate was filtered and dried under vacuum overnight. The crude product was suspended in a minimal amount of $CHCL_3$, sonicated for 10 min, filtered and dried to afford ligand **L12** as a white solid white solid. Yield 1.22 gram 3.33 mmol 33% yield. **Rf** 0.3 (95/5 DCM/MeOH). **^{1}H NMR** (400 MHz, $CDCl_3$) δ 8.79 (d, *j* = 4.7 Hz, 2H), 8.48 (d, *j* = 8.0 Hz, 2H), 8.16 – 8.08 (m, 4H),

7.99 – 7.87 (m, 4H), 7.59 – 7.48 (m, 2H). **^{13}C NMR** (101 MHz, $CDCl_3$) δ 192.80 (C=O), 154.75 (Cq), 154.37 (Cq), 153.52 (Cq), 149.29 (CH), 137.74 (CH), 136.52 (CH), 126.32 (CH), 125.54 (CH), 125.32 (CH), 124.05 (CH). **HR-MS** $[M+H^+]^+$: 367.11895 (calculated) 367.11834 (measured).

2.5.5.9 H_2L13

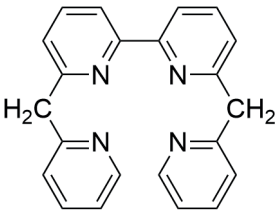

Ligand **L12** (108 mg, 0.30 mmol) was added to a solution of potassium hydroxide (3.14 g, 56 mmol) in diethylene glycol (10 mL). Hydrazine hydrate (3.0 ml, 62 mmol) was added and the solution was refluxed for 4 h. The reaction mixture was allowed to cool and water (100 mL) was added and the solution was extracted with DCM (3x30 mL). The organic layers were combined, dried over magnesium sulfate, filtered and concentrated in vacuo to afford ligand H_2**L13** as a white solid. Yield 106 mg, 0.28 mmol, 98%.

Rf 0.9 (95/5 DCM/MeOH). **^{1}H NMR** (300 MHz, $CDCl_3$) δ 7.82 (s, 2H), 7.54 (d, *j* = 7.8 Hz, 2H), 6.95 (t, *j* = 7.8 Hz, 2H), 6.84 (t, *j* = 7.7 Hz, 2H), 6.57 (d, *j* = 7.8 Hz, 2H), 6.49 (d, *j* = 7.7 Hz, 2H), 6.42 – 6.31 (m, 2H), 3.68 (s, 4H). **^{13}C NMR** (75 MHz, $CDCl_3$) δ 158.39 (Cq), 157.39 (Cq), 154.57 (Cq), 148.02 (CH) , 136.03 (CH), 135.20 (CH), 122.42(CH), 122.08 (CH), 120.16 (CH), 117.61 (CH), 46.13 (CH_2).**HR-MS** $[M+H]^+$: 339.16042 (calculated) 339.15986 (measured).

2.5.5.10 L14

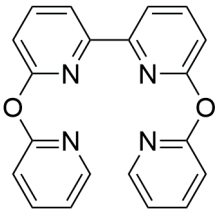

2-Hydroxypyridine (303 mg 3,18 mmol) was dissolved in dry THF (5 mL) and sodium hydride (76.0 mg, 3.18 mmol) was carefully added in portions. The suspension was filtered after the formation of H_2 stopped. The residue and 6,6'-dibromo-2,2'-bipyridine (500 mg, 1,59 mmol) were dissolved in DMSO (15 mL) and the solution was refluxed overnight. Water (15 mL) was added and the suspension was filtered and the crude precipitate was further purified by silica column (100 DCM > 90/10 DCM/MeOH) to afford ligand **L14** as a light brown solid. Yield 314 mg, 0.92 mmol, 57 % **Rf** 0.9 (95/5 DCM/MeOH). **^{1}H NMR** (500 MHz, $CDCl_3$) δ 8.43 (d, *j* = 6.5 Hz, 2H), 8.06 – 7.99 (m, 4H), 7.97 (t, *j* = 7.8 Hz, 2H), 7.44 (ddd, *j* = 8.9, 6.5, 2.1 Hz, 2H), 6.69 (d, *j* = 9.2 Hz, 2H), 6.36 (t, *j* = 6.8 Hz, 2H). **^{13}C NMR** (126 MHz, $CDCl_3$) δ 162.44 (Cq), 154.65 (Cq), 151.38 (Cq), 140.32 (CH), 138.84 (CH), 136.20 (CH), 122.30 (CH), 121.76 (CH), 120.32 (CH), 106.45 (CH). **HR-MS** $[M+H]^+$: 343.11895 (calculated) 343.11835 (measured).

2.5.5.11 [Pt(H_2L2)]$(Cl)_2$

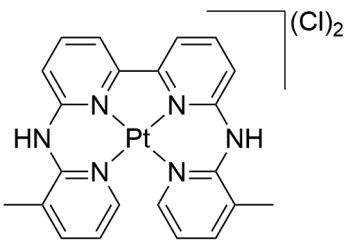

[Pt(MeCN)$_2$(Cl)$_2$] (50 mg, 0.14 mmol) and ligand H_2**L2** (48 mg, 0.13 mmol) were added to DMSO (5 mL) and heated to 110 °C for 15 min as the reaction mixture turned orange. The mixture was allowed to cool to room temperature and the color became bright yellow after addition of 3 M HCl in cyclopentyl methyl ether (1 mL). The mixture was dry-loaded on a column (100 DCM -> 90 DCM 10 MeOH -> 85 DCM 10 MeOH 5 TEA). The green band that was collected last was concentrated in vacuo and dissolved in minimal amount of MeOH (2 mL). The solution was then neutralized by the addition of 3 M HCl in cyclopentyl methyl ether (1 mL). EtOAc was added to precipitate the bright yellow compound [Pt(H_2**L2**)](Cl)$_2$. Yield 56 mg, 0.088 mmol, 68%. **Rf** 0.7 (89/10/1 DCM/MeOH/TEA). **^{1}H NMR** (850 MHz, TFA-d) δ 8.36 (t, *j* = 8.1 Hz, 1H), 8.24 – 8.21 (m, 1H), 8.11 (d, *j* = 7.7 Hz, 1H), 8.06 (d, *j* = 7.3 Hz, 1H), 7.93 (d, *j* = 8.5 Hz, 1H), 7.20 (t, *j* = 6.8 Hz, 1H), 2.76 (s, 3H). **^{13}C NMR** (214 MHz, TFA-d) δ 153.39 (Cq), 147.46 (CH), 146.96 (Cq), 145.85 (Cq), 142.30 (CH), 141.38 (CH), 125.00 (Cq), 120.55 (CH), 117.94 (CH), 116.95 (CH), 16.45 (CH_3). **HR-MS** [M-H-2Cl]$^+$: 562.13153 (calculated) 562.13034 (measured). **Elem. Anal**. Calc. for [$C_{22}H_{20}Cl_2N_6Pt$]: C 41.65; H 3.18; N 13.25. Found: C 41.73; H 3.14; N 13.21.

2.5.5.12 [Pt(H_2L3)]$(Cl)_2$

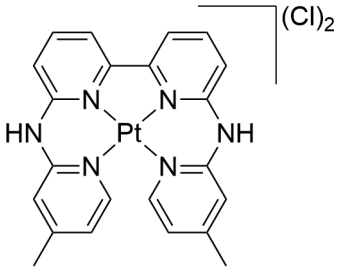

Compound [Pt(H_2**L3**)](Cl)$_2$ was synthesized according the procedure for [Pt(H_2**L2**)](Cl)$_2$. Starting from [Pt(MeCN)$_2$(Cl)$_2$] (0.3 mmol scale), but with ligand H_2**L3** instead of H_2**L2** to afford the bright yellow compound [Pt(H_2**L3**)](Cl)$_2$. Yield 114 mg, 0.18 mmol, 60%. **Rf** 0.5 (94/5/1 DCM/MeOH/TEA). **^{1}H NMR** (850 MHz, TFA-d) δ 8.36 (t, *j* = 8.0 Hz, 1H), 8.19 (d, *j* = 6.5 Hz, 1H), 8.09 (d, *j* = 7.7 Hz, 1H), 7.85 (d, *j* = 8.5 Hz, 1H), 7.60 (s, 1H), 7.14 (dd, *j* = 6.5, 1.8 Hz, 1H), 2.57 (s, 3H). **^{13}C NMR** (214 MHz, TFA-d) δ 158.17 (Cq), 155.64 (Cq), 150.18 (CH), 149.28 (Cq), 143.48 (CH), 124.55 (CH), 119.71 (CH), 118.75 (CH), 118.01 (CH), 21.91 (CH_3). **HR-MS** [M-2Cl]$^{2+}$: 281.56941 (calculated) 281.56902 (measured). **Elem. Anal**. Calc. for [$C_{22}H_{20}Cl_2N_6Pt$]: C 41.65; H 3.18; N 13.25. Found: C 41.38; H 3.16; N 13.18.

2.5.5.13 [Pt(H_2**L4**)]($Cl)_2$

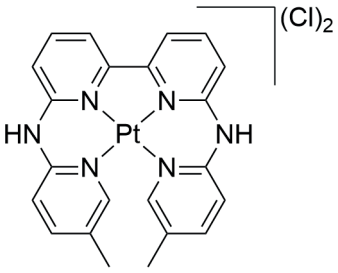

Compound [Pt(H_2**L4**)]($Cl)_2$ was synthesized according the procedure for [Pt(H_2**L2**)]($Cl)_2$. Starting from [Pt($MeCN)_2(Cl)_2$] (0.3 mmol scale), but with ligand H_2**L4** instead of H_2**L2** to afford the bright yellow compound [Pt(H_2**L4**)]($Cl)_2$. Yield 133 mg, 0.21 mmol, 70%. **Rf** 0.5 (94/5/1 DCM/MeOH/TEA). **^{1}H NMR** (850 MHz, TFA-d) δ 8.47 – 8.43 (m, 1H), 8.29 (s, 1H), 8.20 – 8.16 (m, 2H), 7.93 (d, *j* = 8.5 Hz, 1H), 7.81 (d, *j* = 8.6 Hz, 1H), 2.53 (s, 3H). **^{13}C NMR** (214 MHz, TFA-d) δ 155.62 (Cq), 149.79 (CH), 149.15 (Cq), 147.90 (Cq), 145.38 (CH), 143.44 (CH), 134.11 (Cq), 119.66 (CH), 118.66 (CH), 117.99 (CH), 17.80 (CH_3). **HR-MS** $[M-2Cl]^{2+}$: 281.56939 (calculated) 281.56896 (measured). **Elem. Anal**. Calc. for [$C_{22}H_{20}Cl_2N_6Pt$]: C 41.65; H 3.18; N 13.25. Found: C 41.39; H 3.17; N 13.16.

2.5.5.14 [Pt(H_2**L5**)]($Cl)_2$

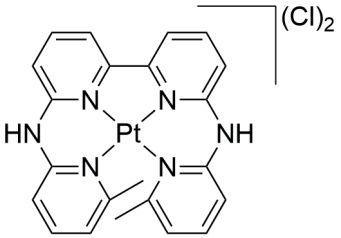

Compound [Pt(H_2**L5**)]($Cl)_2$was synthesized according the procedure for [Pt(H_2**L2**)]($Cl)_2$. Starting from [Pt($MeCN)_2(Cl)_2$] (0.15 mmol scale), but with ligand H_2**L5** instead of H_2**L2** to afford the bright yellow compound [Pt(H_2**L5**)]($Cl)_2$. Yield 63 mg, 0.10 mmol, 67%. **Rf** 0.5 (95/4/1 DCM/MeOH/TEA). **^{1}H NMR** (850 MHz, TFA-d) δ 8.29 (t, *j* = 8.0 Hz, 1H), 8.02 – 7.98 (m, 2H), 7.83 (d, *j* = 8.5 Hz, 1H), 7.63 (d, *j* = 8.3 Hz, 1H), 7.16 (d, *j* = 7.3 Hz, 1H), 2.25 (s, 3H). **^{13}C NMR** (214 MHz, TFA-d) δ 161.30 (Cq), 156.26 (Cq), 151.15 (Cq), 149.43 (Cq), 143.99 (CH), 143.97 (CH), 124.39 (CH), 119.75 (CH), 118.29 (CH), 115.71 (CH), 27.01 (CH_3). **HR-MS** $[M-H-2Cl]^+$: 562.13150 (calculated) 562.13045 (measured). **Elem. Anal**. Calc. for [$C_{22}H_{20}Cl_2N_6Pt$]: C 41.65; H 3.18; N 13.25. Found: C 41.63; H 3.14; N 13.21.

2.5.5.15 [Pt(H_2**L6**)]($Cl)_2$

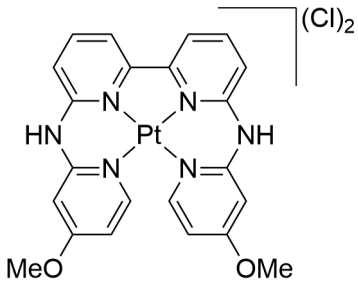

Compound [Pt(H_2**L6**)]($Cl)_2$ was synthesized according the procedure for [Pt(H_2**L2**)]($Cl)_2$. Starting from [Pt($MeCN)_2(Cl)_2$] (0.3 mmol scale), but with ligand H_2**L6** instead of H_2**L2** to afford the bright yellow compound [Pt(H_2**L6**)]($Cl)_2$. Yield 78 mg, 0.12 mmol, 40%. **Rf** 0.6 (94/5/1 DCM/MeOH/TEA). **^{1}H NMR** (850 MHz, TFA-d) δ 8.25 (t, *j* = 8.1 Hz, 1H), 8.03 (d, *j* = 7.2 Hz, 1H), 7.97 (d, *j* = 7.6 Hz, 1H), 7.74 (d, *j* = 8.5 Hz, 1H),

7.15 (d, *j* = 2.7 Hz, 1H), 6.81 (dd, *j* = 7.2, 2.7 Hz, 1H), 4.03 (s, 3H). **^{13}C NMR** (214 MHz, TFA-d) δ 171.80 (Cq), 155.60 (Cq), 151.64 (CH), 151.04 (Cq), 149.45 (Cq), 143.29 (CH), 119.43 (CH), 118.58 (CH), 112.79 (CH), 100.24 (CH), 58.04 (CH_3). **HR-MS** [M-H-2Cl]$^+$: 594.12133 (calculated) 594.12082 (measured). **Elem. Anal**. Calc. for [$C_{22}H_{20}Cl_2N_6O_2Pt$]: C 39.65; H 3.03; N 12.61. Found: C 39.41; H 3.10; N 12.53.

2.5.5.16 [Pt(H_2**L7**)]($Cl)_2$

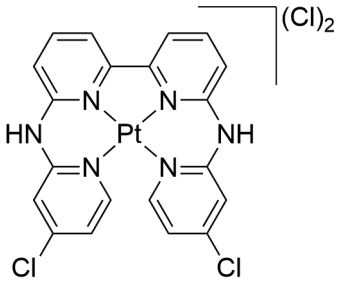

Compound [Pt(H_2**L7**)]($Cl)_2$ was synthesized according the procedure for [Pt(H_2**L2**)]($Cl)_2$. Starting from [Pt($MeCN)_2(Cl)_2$] (0.3 mmol scale), but with ligand H_2**L7** instead of H_2**L2** to afford the bright yellow compound [Pt(H_2**L7**)]($Cl)_2$. Yield 99 mg, 0.15 mmol, 48%. **Rf** 0.7 (97/2/1 DCM/MeOH/TEA). **^{1}H NMR** (850 MHz, TFA-d) δ 8.28 (t, *j* = 8.1 Hz, 1H), 8.18 (d, *j* = 6.8 Hz, 1H), 8.03 (d, *j* = 7.7 Hz, 1H), 7.79 (d, *j* = 8.4 Hz, 1H), 7.75 (t, *j* = 1.8 Hz, 1H), 7.18 (dd, *j* = 6.8, 2.2 Hz, 1H). **^{13}C NMR** (214 MHz, TFA-d) δ 155.52 (Cq), 152.62 (Cq), 151.37 (CH), 149.94 (Cq), 148.79 (Cq), 143.75 (CH), 123.86 (CH), 120.27 (CH), 119.03 (CH), 118.13 (CH). **HR-MS** [M-H-2Cl]$^+$: 602.02234 (calculated) 602.01726 (measured). **Elem. Anal**. Calc. for [$C_{20}H_{14}Cl_4N_6Pt$] + 0.5 H_2O: C 35.11; H 2.21; N 12.28. Found: C 34.84; H 2.11; N 12.11.

2.5.5.17 [Pt(H_2**L8**)]($Cl)_2$

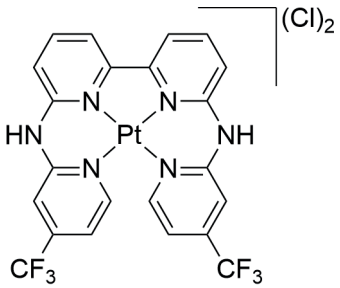

Compound [Pt(H_2**L8**)]($Cl)_2$ was synthesized according the procedure for [Pt(H_2**L2**)]($Cl)_2$. Starting from [Pt($MeCN)_2(Cl)_2$] (0.3 mmol scale), but with ligand H_2**L8** instead of H_2**L2** to afford the bright yellow compound [Pt(H_2**L8**)]($Cl)_2$. Yield 133 mg, 0.18 mmol, 60%. **Rf** 0.7 (94/5/1 DCM/MeOH/TEA). **^{1}H NMR** (850 MHz, TFA-d) δ 8.47 (d, *j* = 6.6 Hz, 1H), 8.35 (t, *j* = 8.0 Hz, 1H), 8.10 (d, *j* = 7.7 Hz, 1H), 8.02 (d, *j* = 1.9 Hz, 1H), 7.90 (d, *j* = 8.4 Hz, 1H), 7.36 (d, *j* = 6.6 Hz, 1H). **^{13}C NMR** (214 MHz, TFA-d) δ 155.45 (Cq), 152.55 (CH), 150.50 (Cq), 148.49 Cq), 145.80(q), 144.08 (CH), 123.13(q), 120.77 (CH), 119.29 (CH), 118.45 (CH), 115.80 (CH). **^{19}F NMR** (471 MHz, TFA-d) δ -68.16. **HR-MS** [M-H-2Cl]$^+$: 670.07496 (calculated) 670.07495 (measured). **Elem. Anal**. Calc. for [$C_{22}H_{14}Cl_2F_6N_6Pt$] + H_2O: C 34.75; H 2.12; N 11.05. Found: C 34.36; H 1.92; N 10.89.

2.5.5.18 $[Pt(H_2L9)](Cl)_2$

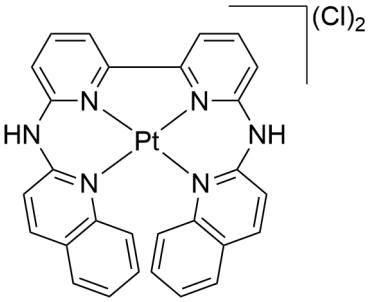

Compound $[Pt(H_2$**L9**$)](Cl)_2$ was synthesized according the procedure for $[Pt(H_2$**L2**$)](Cl)_2$. Starting from $[Pt(MeCN)_2(Cl)_2]$ (0.3 mmol scale), but with ligand H_2**L9** instead of H_2**L2** to afford the bright yellow compound $[Pt(H_2$**L9**$)](Cl)_2$. Yield 124 mg, 0.19 mmol, 64%. **Rf** 0.5 (98/2/1 DCM/MeOH/TEA). **^{1}H NMR** (850 MHz, TFA-d) δ 8.36 (t, *j* = 8.0 Hz, 1H), 8.24 (d, *j* = 8.7 Hz, 1H), 8.10 (d, *j* = 7.6 Hz, 1H), 7.96 (d, *j* = 8.4 Hz, 1H), 7.72 (d, *j* = 8.6 Hz, 1H), 7.68 (d, *j* = 8.7 Hz, 1H), 7.46 (d, *j* = 6.5 Hz, 1H), 7.08 (t, *j* = 7.4 Hz, 1H), 7.01 (t, *j* = 7.1 Hz, 1H). **^{13}C NMR** (214 MHz, TFA-d) δ 156.12 (Cq), 151.11 (Cq), 148.63 (Cq), 147.09 (Cq), 144.53 (CH), 143.70 (CH), 132.82 (CH), 130.15 (CH), 129.32 (CH), 128.52 (Cq), 126.06 (CH), 120.64 (CH), 119.20 (CH), 116.36 (CH). **HR-MS** $[M\text{-}H\text{-}2Cl+3HCN]^+$: 715.16423 (calculated) 715.16376 (measured). **Elem. Anal**. Calc. for $[C_{28}H_{20}Cl_2N_6Pt]$: C 47.60; H 2.85; N 11.90. Found: C 47.42; H 2.79; N 11.83.

2.5.5.19 $[Pt(L10)](PF_6)_2$

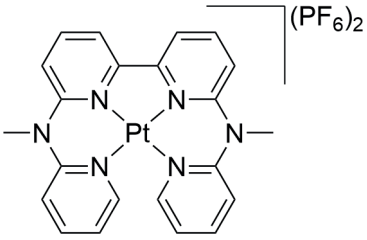

$[Pt(MeCN)_2(Cl)_2]$ (51mg, 0.14 mmol) and **L10** (46 mg, 0.13 mmol) were dissolved in DMSO (5 mL) and heated to 110 °C for 15 min and became orange. The reaction was then precipitated by addition saturated aqueous KPF_6 (5 mL) and washed with H_2O (2x 20 mL) and dried in vacuo overnight to afford the orange compound $[Pt($**L10**$)](Cl)_2$. yield 43 mg, 0.05 mmol, 39%. **^{1}H NMR** (850 MHz, DMSO-d6) δ 8.61 (d, *j* = 4.4 Hz, 1H), 8.55 (t, *j* = 8.1 Hz, 1H), 8.51 (d, *j* = 7.6 Hz, 1H), 8.38 (t, *j* = 7.1 Hz, 1H), 7.94 (dd, *j* = 8.6, 4.3 Hz, 2H), 7.45 (t, *j* = 6.6 Hz, 1H), 3.89 (s, 3H). **^{13}C NMR** (214 MHz, DMSO-d6) δ 154.31 (Cq), 151.26 (Cq), 151.09 (Cq), 151.01 (CH), 142.64 (CH), 142.41 (CH), 122.35 (CH), 119.01 (CH), 118.77 (CH), 117.86 (CH), 42.90 (CH_3). **HR-MS** $[M\text{-}H\text{-}2PF_6+2HCN]^+$: 616.15328 (calculated) 616.15271 (measured). **Elem. Anal**. Calc. for $[C_{22}H_{20}F_{12}P_2N_6Pt]$: C 30.96; H 2.36; N 9.85. Found: C 31.01; H 2.33; N 9.81.

2.5.5.20 [Pt(L11)](PF$_6$)$_2$

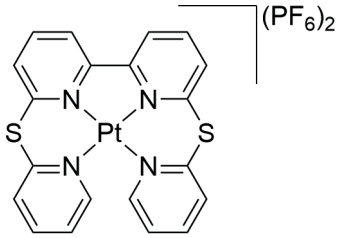

Compound [Pt(**L11**)](PF$_6$)$_2$ was synthesized according the procedure for [Pt(**L10**)](PF$_6$)$_2$. Starting from [Pt(MeCN)$_2$(Cl)$_2$] (0.28 mmol scale), but with ligand **L11** instead of **L10** to afford the bright yellow compound [Pt(H$_2$**L11**)](PF$_6$)$_2$. Yield 170 mg, 0.20 mmol, 71%. **^{1}H NMR** (850 MHz, DMSO) δ 8.81 (t, *j* = 7.4 Hz, 2H), 8.59 (td, *j* = 7.9, 1.9 Hz, 1H), 8.46 (d, *j* = 8.1 Hz, 1H), 8.38 (t, *j* = 7.7 Hz, 1H), 7.62 (t, *j* = 6.8 Hz, 1H). **^{13}C NMR** (214 MHz, DMSO-d6) δ 158.70 (Cq), 156.54 (CH), 151.24 (Cq), 150.68 (Cq), 143.42 (CH), 142.59 (CH), 128.27 (CH), 127.87 (CH), 127.17 (CH), 124.46 (CH). **HR-MS** [M-2PF$_6$+MeO]$^+$: 600.04860 (calculated) 600.04827 (measured). **Elem. Anal**. Calc. for [C$_{20}$H$_{14}$F$_{12}$N$_4$P$_2$PtS$_2$]: C 27.95; H 1.64; N 6.52. Found: C 27.79; H 1.60; N 6.49.

2.5.5.21 [Pt(L12)](Cl)$_2$

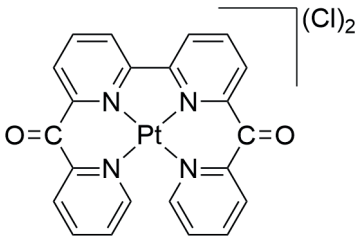

Pt(MeCN)$_2$(Cl)$_2$ (53mg, 0.15 mmol) and **L12** (51 mg, 0.14 mmol) were added to DMF (5 mL) and heated to 110 °C for 15 min and the reaction mixture became orange. The reaction mixture was precipitated by addition EtOAc (10 mL) and filtered. The solid was washed with diethyl ether (2x 25 mL) and vacuum dried overnight to afford the orange compound [Pt(**L12**)](Cl)$_2$. Yield 53 mg, 0.06 mmol, 45% yield. **^{1}H NMR** (850 MHz, DMSO-d6) δ 9.15 (d, *j* = 6.8 Hz, 1H), 8.85 (t, *j* = 7.9 Hz, 1H), 8.75 (d, *j* = 8.0 Hz, 1H), 8.63 (t, *j* = 7.7 Hz, 1H), 8.57 (d, *j* = 6.3 Hz, 1H), 8.54 (d, *j* = 5.7 Hz, 1H), 8.02 (ddd, *j* = 7.5, 5.8, 1.7 Hz, 1H). **^{13}C NMR** (214 MHz, DMSO-d6) δ 184.01 (Cq), 156.28 (Cq), 153.92 (CH), 148.63 (Cq), 147.66 (Cq), 143.94 (CH), 143.12 (CH), 131.37 (CH), 129.86 (CH), 129.38 (CH), 129.34 (CH). **HR-MS** [M-H-2Cl+2HCN]$^+$: 614.09004 (calculated) 614.08491 (measured). **Elem. Anal**. Calc. for [M]: C 41.79; H 2.23; N 8.86. Found: C 41.11; H 2.27; N 8.71.

2.5.5.22 [Pt(H$_2$L13)](PF$_6$)$_2$

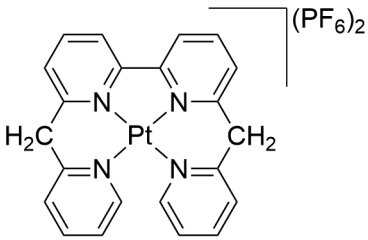

[Pt(MeCN)$_2$(Cl)$_2$] (107mg, 0.31 mmol) and H$_2$**L13** (94 mg, 0.28 mmol) were added to DMF (5 mL) and heated to 110 °C for 15 min. The reaction was precipitated by addition HPF$_6$ (55% in H$_2$O, 5 drops) and further diluted with H$_2$O (15 mL). The precipitate was filtered, washed with H$_2$O (2x 25 mL), and dried overnight in vacuo to afford compound [Pt(H$_2$**L13**)]

$(PF_6)_2$. Yield 136 mg, 0.17 mmol, 55% **^{1}H NMR** (600 MHz, DMSO-d6) δ 8.73 (d, *j* = 6.0 Hz, 2H), 8.69 (d, *j* = 8.1 Hz, 2H), 8.54 (t, *j* = 7.9 Hz, 2H), 8.38 (t, *j* = 7.8 Hz, 2H), 8.10 – 8.04 (m, 4H), 7.70 (t, *j* = 6.9 Hz, 2H), 5.10 (s, 1H).
^{13}C NMR (151 MHz, DMSO-d6) δ 158.12 (Cq), 156.29 (Cq), 155.87 (Cq), 154.94 (CH), 144.44 (CH), 143.48 (CH), 129.20 (CH), 128.21 (CH), 127.50 (CH), 124.48 (CH). **HR-MS** $[M\text{-}H\text{-}2PF_6+2HCN]^+$: 586.13151 (calculated) 586.13068 (measured). **Elem. Anal**. Calc. for $[C_{22}H_{18}F_{12}N_4P_2Pt]$: C 32.09; H 2.20; N 6.80. Found: C 31.89; H 2.19; N 6.74.

2.5.5.23 $[Pd(H_2L2)](Cl)_2$

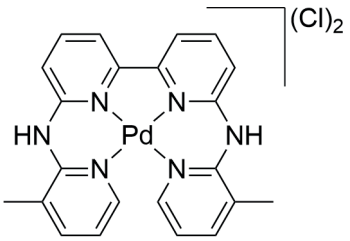

$[Pd(cod)(Cl)_2]$ (101 mg, 0.35 mmol) and ligand H_2**L2** (117 mg, 0.32 mmol) were added to DMSO (5 mL) and heated to 110 °C for 15 min as the reaction mixture turned orange. The mixture was allowed to cool to room temperature and the color became bright yellow after addition of 3 M HCl in cyclopentyl methyl ether (1 mL). The mixture was dry-loaded on a column (100 DCM -> 90 DCM 10 MeOH -> 85 DCM 10 MeOH 5 TEA). The green band that was collected last was concentrated in vacuo and dissolved in minimal amount of MeOH (2 mL). The solution was then neutralized by the addition of HCl in cyclopentyl methyl ether (3 M, 1 mL). EtOAc 20 (mL) was added to precipitate the bright yellow compound $[Pd(H_2$**L2**$)](Cl)_2$. Yield 125 mg, 0.23 mmol, 66%. **Rf** 0.9 (89/10/1 DCM/MeOH/TEA). **^{1}H NMR** (500 MHz, D2O) δ 8.14 (t, *j* = 7.7 Hz, 2H, A4), 7.98 (d, *j* = 7.4 Hz, 2H), 7.93 (d, *j* = 7.8 Hz, 4H), 7.67 (d, *j* = 8.5 Hz, 2H), 7.14 (dd, *j* = 7.3, 6.2 Hz, 2H), 2.56 (s, 6H, CH3). **^{13}C NMR** (126 MHz, D2O) δ 153.75 (Cq), 147.49 (Cq), 147.32 (CH), 145.86 (Cq), 142.94 (CH), 142.02 (CH), 124.93 (Cq), 120.63 (CH), 117.62 (CH), 116.91 (CH), 17.66 (CH_3). **ES-MS** $[M\text{-}H\text{-}2Cl]^+$: 473.1 (calculated) 473.0 (measured). **Elem. Anal**. Calc. for $[C_{22}H_{20}Cl_2N_6Pd] + 0.7\ H_2O$: C 47.32; H 3.86; N 15.05. Found: C 47.11; H 3.79; N 15.00.

2.5.5.24 $[Pd(H_2L3)](Cl)_2$

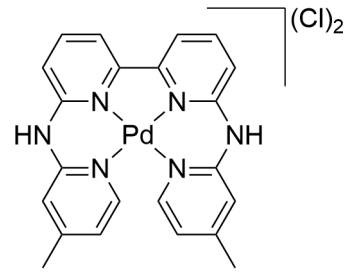

$[Pd(H_2$**L3**$)](Cl)_2$ was synthesized according the procedure for $[Pd(H_2$**L2**$)](Cl)_2$. Starting from $[Pd(cod)(Cl)_2]$ (0.35 mmol scale), but with ligand H_2**L3** instead of H_2**L2** to afford the bright yellow compound $[Pd(H_2$**L3**$)](Cl)_2$. Yield 134 mg, 0.25 mmol, 71%. **Rf** 0.7 (89/10/1 DCM/MeOH/TEA). **^{1}H NMR** (500 MHz, D2O) δ 8.00 (t, *j* = 8.5 Hz, 1H), 7.71 (d, *j* = 6.8 Hz, 1H), 7.67 (d, *j* = 6.4 Hz, 1H), 7.25 (d, *j* = 7.5 Hz, 0H), 7.12 (s, 1H), 6.96 (dd, *j* = 6.4, 1.5 Hz, 1H), 2.40 (s, 3H). **^{13}C NMR** (126 MHz, D2O) δ 155.71 (Cq), 153.23 (Cq), 147.79 (CH), 146.93 (Cq), 146.68 (Cq), 142.22 (CH), 122.32 (CH), 117.36 (CH), 116.07 (CH), 115.15 (CH), 20.58 (CH_3). **HR-MS** $[M\text{-}2Cl]^{2+}$: 237.03867 (calculated) 237.03863

(measured). **Elem. Anal**. Calc. for [$C_{22}H_{20}Cl_2N_6Pd$]: C 48.42; H 3.69; N 15.40. Found: C 48.18; H 3.89; N 15.26.

2.5.5.25 [Pd(H_2**L4**)]($Cl)_2$

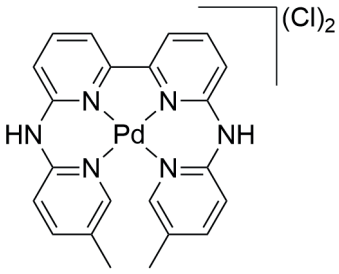

Compound [Pd(H_2**L4**)]($Cl)_2$ was synthesized according the procedure for [Pd(H_2**L2**)]($Cl)_2$. Starting from [Pd(cod)($Cl)_2$] (0.35 mmol scale), but with ligand H_2**L4** instead of H_2**L2** to afford the bright yellow compound [Pd(H_2**L4**)]($Cl)_2$. Yield 108 mg, 0.20 mmol, 57%. **Rf** 0.7 (89/10/1 DCM/MeOH/TEA). **^{1}H NMR** (500 MHz, D2O) δ 7.97 (t, *j* = 8.5 Hz, 1H), 7.89 (dd, *j* = 8.5, 1.5 Hz, 1H), 7.68 (d, *j* = 6.8 Hz, 1H), 7.62 (s, 1H), 7.24 – 7.17 (m, 2H), 2.07 (s, 3H). **^{13}C NMR** (126 MHz, D2O) δ 153.12 (Cq), 147.02 (CH), 146.64 (Cq), 145.24 (Cq), 143.91 (CH), 142.19 (CH), 131.23 (Cq), 117.38 (CH), 116.04 (CH), 115.28 (CH), 16.62 (CH_3). **HR-MS** [M-2Cl]$^{2+}$: 237.03867 (calculated) 237.03866 (measured). **Elem. Anal**. Calc. for [$C_{22}H_{20}Cl_2N_6Pd$] + 3 H_2O: C 44.06; H 4.37; N 14.01. Found: C 44.41; H 4.01; N 13.91.

2.5.5.26 [Pd(H_2**L5**)]($Cl)_2$

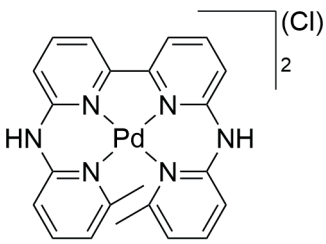

Compound [Pd(H_2**L5**)]($Cl)_2$ was synthesized according the procedure for [Pd(H_2**L2**)]($Cl)_2$. Starting from [Pd(cod)($Cl)_2$] (0.35 mmol scale), but with ligand H_2**L5** instead of H_2**L2** to afford the bright yellow compound [Pd(H_2**L5**)]($Cl)_2$. Yield 77 mg, 0.14 mmol, 40%. **Rf** 0.7 (89/10/1 DCM/MeOH/TEA). **^{1}H NMR** (500 MHz, D2O) δ 8.05 (t, *j* = 8.5, Hz, 1H), 7.86 (t, *j* = 8.4 Hz, 1H), 7.75 (d, *j* = 6.7 Hz, 1H), 7.33 (d, *j* = 7.5 Hz, 1H), 7.23 (d, *j* = 8.4 Hz, 1H), 7.05 (d, *j* = 6.7 Hz, 1H), 2.05 (s, 3H). **^{13}C NMR** (126 MHz, D2O) δ 157.70 (Cq), 154.46 (Cq), 148.08 (Cq), 147.18 (Cq), 142.26 (CH), 142.14 (CH), 121.86 (CH), 117.30 (CH), 115.70 (CH), 113.04 (CH), 25.44 (CH_3). **HR-MS** [M-2Cl]$^{2+}$: 237.03867 (calculated) 237.03869 (measured). **Elem. Anal**. Calc. for [$C_{22}H_{20}Cl_2N_6Pd$] + H_2O: C 46.87; H 3.93; N 14.91. Found: C 46.81; H 3.89; N 14.87.

2.5.5.27 $[Pd(H_2L6)](Cl)_2$

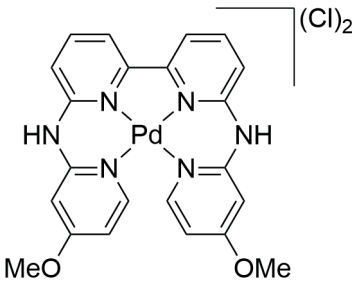

Compound $[Pd(H_2\mathbf{L6})](Cl)_2$ was synthesized according the procedure for $[Pd(H_2\mathbf{L2})](Cl)_2$. Starting from $[Pd(cod)(Cl)_2]$ (0.35 mmol scale), but with ligand $H_2\mathbf{L6}$ instead of $H_2\mathbf{L2}$ to afford the bright yellow compound $[Pd(H_2\mathbf{L6})](Cl)_2$. Yield 96 mg, 0.17 mmol, 52%. **Rf** 0.5 (94/5/1 DCM/MeOH/TEA). **^{1}H NMR** (500 MHz, D2O) δ 7.97 (dd, *j* = 8.5, 7.6 Hz, 1H), 7.66 (t, *j* = 6.9Hz, 2H), 7.20 (d, *j* = 7.5 Hz, 1H), 6.72 (dd, *j* = 7.1, 2.7 Hz, 1H), 6.69 (d, *j* = 2.7 Hz, 1H), 3.91 (s, 3H). **^{13}C NMR** (126 MHz, D2O) δ 169.27 (Cq), 153.19 (Cq), 149.65 (CH), 148.56 (Cq), 147.12 (Cq), 142.17 (CH), 117.22 (CH), 116.02 (CH), 110.07 (CH), 98.10 (CH), 56.83 (CH_3). **HR-MS** $[M\text{-}2Cl]^{2+}$: 253.03358 (calculated) 253.03349 (measured). **Elem. Anal**. Calc. for $[C_{22}H_{20}Cl_2N_6O_2Pd]$ + 0.6 H_2O: C 44.90; H 3.63; N 14.28. Found: C 44.84; H 3.53; N 14.12.

2.5.5.28 $[Pd(H_2L7)](Cl)_2$

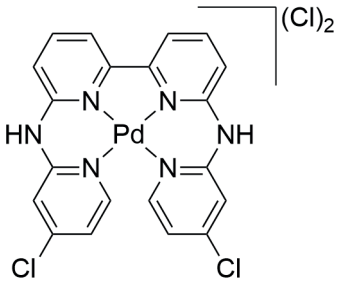

Compound $[Pd(H_2\mathbf{L7})](Cl)_2$was synthesized according the procedure for $[Pd(H_2\mathbf{L2})](Cl)_2$. Starting from $[Pd(cod)(Cl)_2]$ (0.35 mmol scale), but with ligand $H_2\mathbf{L7}$ instead of $H_2\mathbf{L2}$ to afford the bright yellow compound $[Pd(H_2\mathbf{L7})](Cl)_2$. Yield 78 mg, 0.14 mmol, 41%. **Rf** 0.5 (97/2/1 DCM/MeOH/TEA). **^{1}H NMR** (850 MHz, TFA-d) δ 8.24 (t, *j* = 8.0 Hz, 1H), 8.07 (d, *j* = 6.6 Hz, 2H), 7.99 (d, *j* = 7.6 Hz, 1H), 7.72 (d, *j* = 8.4 Hz, 1H), 7.69 (s, 1H), 7.26 (d, *j* = 4.5 Hz, 1H). **^{13}C NMR** (214 MHz, TFA-d) δ 156.29 (Cq), 153.46 (Cq), 151.23 (CH), 150.24 (Cq), 149.56 (Cq), 144.53 (CH), 123.77 (CH), 119.93 (CH), 119.03 (CH), 117.92 (CH). **HR-MS** $[M\text{-}2Cl]^{2+}$: 257.98402 (calculated) 257.98300 (measured). **Elem. Anal**. Calc. for $[C_{20}H_{14}Cl_4N_6Pd]$ + 0.4 HCl: C 39.96; H 2.41; N 13.98. Found: C 40.11; H 2.39; N 13.98.

2.5.5.29 $[Pd(H_2L8)](Cl)_2$

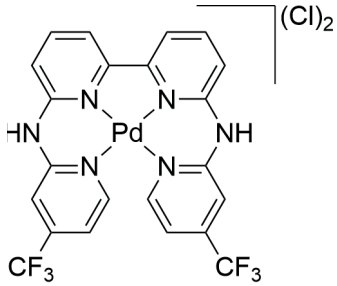

Compound $[Pd(H_2\mathbf{L8})](Cl)_2$ was synthesized according the procedure for $[Pd(H_2\mathbf{L2})](Cl)_2$. Starting from $[Pd(cod)(Cl)_2]$ (0.18 mmol scale), but with ligand $H_2\mathbf{L8}$ instead of $H_2\mathbf{L2}$ to afford the bright yellow compound $[Pd(H_2\mathbf{L8})](Cl)_2$. Yield 42 mg, 0.06 mmol, 36%. **Rf** 0.8 (97/2/1 DCM/MeOH/TEA). **^{1}H NMR** (850 MHz, TFA-d) δ 8.39 (d, *j* = 6.5 Hz, 1H), 8.31 (t, *j* = 8.0 Hz, 1H), 8.07 (d, *j* = 7.6 Hz, 1H), 7.96 (s, 1H), 7.81 (d, *j* = 8.4 Hz, 1H), 7.46 (d, *j* = 4.7 Hz, 1H). **^{13}C NMR** (214 MHz, TFA-d) δ 156.35

(Cq), 152.47 (CH), 150.74 (Cq), 149.23 (Cq), 146.63 (q, *j* = 36.6 Hz), 144.80 (CH), 123.23 (q, *j* = 273.2 Hz), 120.46 (CH), 119.27 (CH), 118.27 (CH), 115.31 (CH), 115.29 (CH). **^{19}F NMR** (471 MHz, TFA-d) δ -66.69. **HR-MS** [[M-H-2Cl]$^{+}$: 581.01361 (calculated) 581.01422 (measured). **Elem. Anal**. Calc. for [$C_{22}H_{14}Cl_2F_6N_6Pd$]: C 40.42; H 2.16; N 12.86. Found: C 39.95; H 2.26; N 12.69.

2.5.5.30 [Pd(H_2L9)]($Cl)_2$

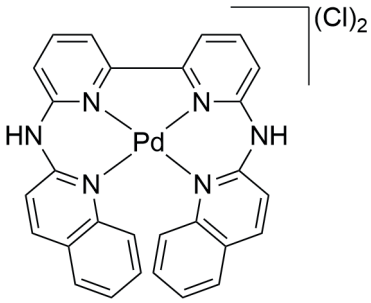

Compound [Pd(H_2**L9**)]($Cl)_2$ was synthesized according the procedure for [Pd(H_2**L2**)]($Cl)_2$. Starting from [Pd(cod)($Cl)_2$] (0.35 mmol scale), but with ligand H_2**L9** instead of H_2**L2** to afford the bright yellow compound [Pd(H_2**L9**)]($Cl)_2$. Yield 111 mg, 0.18 mmol, 51% **Rf** 0.7 (94/5/1 DCM/MeOH/TEA). **^{1}H NMR** (500 MHz, TFA-d) δ 8.41 (t, *j* = 7.9 Hz, 1H), 8.32 (d, *j* = 8.6 Hz, 1H), 8.18 (d, *j* = 7.6 Hz, 1H), 7.93 (d, *j* = 8.4 Hz, 1H), 7.76 (d, *j* = 8.5 Hz, 1H), 7.68 (d, *j* = 8.8 Hz, 1H), 7.54 (d, *j* = 8.0 Hz, 1H), 7.21 (t, *j* = 7.5 Hz, 1H), 7.09 (t, *j* = 7.9 Hz, 1H). **^{13}C NM**R (126 MHz, TFA-d) δ **^{13}C NMR** (126 MHz, TFA-d) δ 155.17 (Cq), 148.89 (Cq), 147.05 (Cq), 144.44 (Cq), 142.74 (two peaks, CH), 130.71 (CH), 128.04 (CH), 126.89 (CH), 126.30 (Cq), 123.71 (CH), 118.65 (CH), 117.22 (CH), 114.09 (CH). **HR-MS** [M-H-2Cl]$^{2+}$: 545.07110 (calculated) 545.07011 (measured). **Elem. Anal**. Calc. for [$C_{28}H_{20}Cl_2N_6Pd$] + 0.7 H_2O: C 53.35; H 3.42; N 13.33. Found: C 53.31; H 3.48; N 13.21.

2.5.5.31 [Pd(L10)]($Cl)_2$

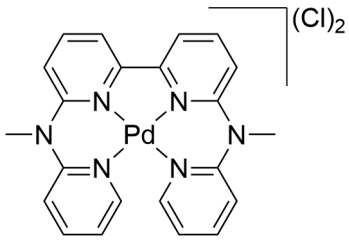

[Pd(cod)($Cl)_2$] (75 mg, 0.26 mmol) and **L10** (97 mg, 0.26 mmol) were added to $CHCl_3$ (15 mL) and refluxed for 3 h. The precipitate was filtered and washed with EtOAc (3x 10 mL) and DCM (50 mL). The solid was vacuum dried overnight to afford the orange/yellow compound [Pt(**L10**)]($Cl)_2$. Yield 87 mg, 0.18 mmol, 71% yield. **^{1}H NMR** (500 MHz, DMSO-d6) δ 8.51 – 8.43 (m, 3H), 8.34 (ddd, *j* = 8.8, 7.2, 1.7 Hz, 1H), 7.86 (t, *j* = 8.1 Hz, 2H), 7.48 (t, *j* = 7.2 Hz, 1H), 3.85 (s, 3H). **^{13}C NMR** (126 MHz, DMSO-d6) δ 154.86 (Cq), 151.45 (Cq), 151.31 (Cq), 150.74 (CH), 143.19 (CH), 142.97 (CH), 122.21 (CH), 118.91 (CH), 118.53 (CH), 117.92 (CH), 42.65 (CH_3). **HR-MS** [M-2Cl]$^{2+}$: 237.03867 (calculated) 237.03863 (measured). **Elem. Anal**. Calc. for [$C_{22}H_{20}Cl_2N_6Pd$] + 0.4 DCM: C 46.41; H 3.62; N 14.50. Found: C 46.36; H 3.63; N 14.37.

2.5.5.32 [Pd(L11)](PF$_6$)$_2$

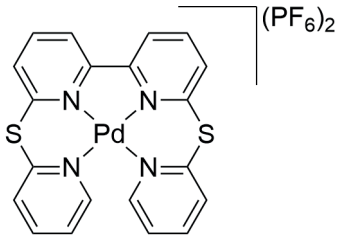

[Pd(cod)(Cl)$_2$] (100 mg, 0.35 mmol) and **L10** (117 mg, 0.32 mmol) were dissolved in DMSO (5 mL) and heated to 110 °C for 15 min and became orange. The reaction was then precipitated by addition saturated aqueous KPF$_6$ (5 mL) and washed with H$_2$O (2x 20 mL) and dried in vacuo overnight to afford the orange compound [Pt(**L11**)](PF$_6$)$_2$. yield 119 mg, 0.16 mmol, 50%. **^{1}H NMR** (600 MHz, DMSO-d6) δ 8.73 (d, *j* = 7.9 Hz, 1H), 8.69 (d, *j* = 7.3 Hz, 0H), 8.54 (t, *j* = 8.0 Hz, 1H), 8.37 – 8.29 (m, 3H), 7.64 (ddd, *j* = 7.5, 6.1, 1.9 Hz, 1H). **^{13}C NMR** (151 MHz, DMSO-d6) δ 157.90, 156.15, 156.05, 155.47, 155.34, 154.84, 150.92, 150.25, 142.89, 142.18, 138.84, 137.78, 127.60, 127.37, 126.28, 126.14, 125.68, 124.66, 124.28, 123.92, 122.54, 118.55. **Elem. Anal**. Calc. for [$C_{20}H_{14}F_{12}N_4P_2PdS_2$]: C 31.16; H 1.83; N 7.27. Found: C 31.26; H 1.81; N 7.25.

2.5.5.33 [Pd(L12)](Cl)$_2$

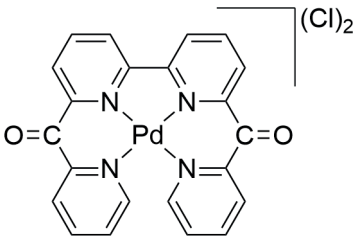

[Pd(cod)(Cl)$_2$] (52 mg, 0.19 mmol) and **L12** (63 mg, 0.17 mmol) were added to DMF (5 mL) and heated to 110 °C for 15 min and the reaction mixture became orange. The reaction mixture was precipitated by addition EtOAc (10 mL) and filtered. The solid was washed with diethyl ether (2x 25 mL) and vacuum dried overnight to afford the orange compound [Pd(**L12**)](Cl)$_2$. Yield 40 mg, 0.07 mmol, 43% yield. **^{1}H NMR** (850 MHz, DMSO-d6) δ 9.12 (dd, *j* = 8.1, 1.3 Hz, 6H), 8.82 (t, *j* = 7.9 Hz, 7H), 8.74 (d, *j* = 4.7 Hz, 2H), 8.70 (d, *j* = 9.1 Hz, 4H), 8.55 (t, *j* = 7.0 Hz, 3H), 8.51 – 8.48 (m, 13H), 8.35 (d, *j* = 6.9 Hz, 1H), 8.16 (t, *j* = 7.8 Hz, 2H), 8.13 – 8.08 (m, 4H), 8.04 (d, *j* = 6.6 Hz, 1H), 8.00 (ddd, *j* = 7.4, 5.6, 1.7 Hz, 7H), 7.73 – 7.68 (m, 2H). **^{13}C NMR** (214 MHz, DMSO-d6) δ 193.60, 183.96, 156.16, 154.45, 154.38, 154.35, 153.48, 149.57, 148.52, 147.03, 144.15, 142.99, 138.98, 137.69, 130.87, 129.81, 129.20, 128.97, 127.45, 125.45, 125.11, 123.97, 123.63. **Elem. Anal**. Calc. for [$C_{22}H_{14}Cl_2N_4O_2Pd$] + 0.6 HCl: C 46.72; H 2.60; N 9.91. Found: C 46.19; H 2.41; N 10.11.

2.5.5.34 [Pd(H_2L13)]($Cl)_2$

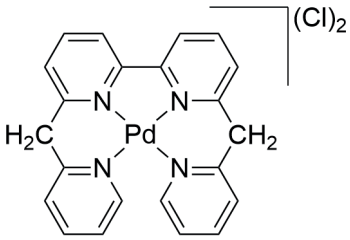

[Pd(cod)($Cl)_2$] (60 mg, 0.21 mmol) and H_2**L13** (71 mg, 0.21 mmol) were added to $CHCl_3$ (15 mL) and refluxed for 3 h. The precipitate was filtered and washed with EtOAc (3x 10 mL) and diethylether (50 mL). The solid was vacuum dried overnight to afford the orange/yellow compound [Pt(H_2**L13**)]($Cl)_2$. Yield 88 mg, 0.17 mmol, 81% **^{1}H NMR** (600 MHz, DMSO-d6) δ 8.70 – 8.65 (m, 2H), 8.51 (t, *j* = 7.9 Hz, 1H), 8.36 – 8.30 (m, 1H), 8.04 (dd, *j* = 7.8, 1.2 Hz, 1H), 8.00 (dd, *j* = 7.9, 1.5 Hz, 1H), 7.71 (ddd, *j* = 7.5, 5.8, 1.5 Hz, 1H), 5.18 (s, 2H). **^{13}C NMR** (151 MHz, DMSO-d6) δ 156.67 (Cq), 155.27 (Cq), 155.25 (Cq), 153.72 (Cq), 153.70 (Cq), 153.47 (CH), 143.28 (CH), 142.27 (CH), 127.95 (CH), 126.72 (CH), 125.74 (CH), 123.11 (CH). **HR-MS** [M-H-2Cl]$^+$: 443.04838 (calculated) 443.04856 (measured). **Elem. Anal**. Calc. for [$C_{22}H_{18}N_4Pd$]: C 51.24; H 3.52; N 10.86. Found: C 50.79; H 3.49; N 10.81.

2.6 Literature

(1) Rosenberg, B.; Van Camp, L.; Krigas, T. Inhibition of Cell Division in Escherichia Coli by Electrolysis Products from a Platinum Electrode. *Nature* **1965**, *205* (4972), 698–699.

(2) Cohen, S. M.; Lippard, S. J. Cisplatin: From DNA Damage to Cancer Chemotherapy. In *Progress in Nucleic Acid Research and Molecular Biology*; Academic Press, 2001; Vol. 67, pp 93–130.

(3) Todd, R. C.; Lippard, S. J. Inhibition of Transcription by Platinum Antitumor Compounds. *Metallomics* **2009**, *1* (4), 280–291.

(4) Jung, Y.; Lippard, S. J. Direct Cellular Responses to Platinum-Induced DNA Damage. *Chem. Rev.* **2007**, *107* (5), 1387–1407.

(5) Khoury, A.; Deo, K. M.; Aldrich-Wright, J. R. Recent Advances in Platinum-Based Chemotherapeutics That Exhibit Inhibitory and Targeted Mechanisms of Action. *J. Inorg. Biochem.* **2020**, *207*, 111070.

(6) Kelland, L. The Resurgence of Platinum-Based Cancer Chemotherapy. *Nat. Rev. Cancer* **2007**, *7* (8), 573–584.

(7) Hope, J. M.; Wilson, J. J.; Lippard, S. J. Photoluminescent DNA Binding and Cytotoxic Activity of a Platinum(Ii) Complex Bearing a Tetradentate β-Diketiminate Ligand. *Dalton Trans.* **2013**, *42* (9), 3176–3180.

(8) Hooper, C. A. J.; Cardo, L.; Craig, J. S.; Melidis, L.; Garai, A.; Egan, R. T.; Sadovnikova, V.; Burkert, F.; Male, L.; Hodges, N. J.; Browning, D. F.; Rosas, R.; Liu, F.; Rocha, F. V.; Lima, M. A.; Liu, S.; Bardelang, D.; Hannon, M. J. Rotaxanating Metallo-Supramolecular Nano-Cylinder Helicates to Switch DNA Junction Binding. *J. Am. Chem. Soc.* **2020**, *142* (49), 20651–20660.

(9) Harper, B. W. J.; Morris, T. T.; Gailer, J.; Aldrich-Wright, J. R. Probing the Interaction of Bisintercalating (2,2′:6′,2″-Terpyridine)Platinum(II) Complexes with Glutathione and Rabbit Plasma. *J. Inorg. Biochem.* **2016**, *163*, 95–102.

(10) Pages, B. J.; Sakoff, J.; Gilbert, J.; Zhang, Y.; Kelly, S. M.; Hoeschele, J. D.; Aldrich-Wright, J. R. Combining the Platinum(Ii) Drug Candidate Kiteplatin with 1,10-Phenanthroline Analogues. *Dalton Trans.* **2018**, *47* (7), 2156–2163.

(11) Cusumano, M.; Di Pietro, M. L.; Giannetto, A.; Vainiglia, P. A. The Intercalation to DNA of Bipyridyl Complexes of Platinum(II) with Thioureas. *J. Inorg. Biochem.* **2005**, *99* (2), 560–565.

(12) Shahabadi, N.; Mohammadi, S.; Alizadeh, R. DNA Interaction Studies of a New Platinum(II) Complex Containing Different Aromatic Dinitrogen Ligands. *Bioinorg. Chem. Appl.* **2011**, *2011*, 429241.

(13) Mukherjee, T.; Sen, B.; Zangrando, E.; Hundal, G.; Chattopadhyay, B.; Chattopadhyay, P. Palladium(II) and Platinum(II) Complexes of Deprotonated N,N′-Bis(2-Pyridinecarboxamide)-1,2-Benzene: Synthesis, Structural Characterization and Binding Interactions with DNA and BSA. *Inorganica Chim. Acta* **2013**, *406*, 176–183.

(14) Liu, H.-K.; Sadler, P. J. Metal Complexes as DNA Intercalators. *Acc. Chem. Res.* **2011**, *44* (5), 349–359.

(15) Reinhardt, C. G.; Krugh, T. R. A Comparative Study of Ethidium Bromide Complexes with Dinucleotides and DNA: Direct Evidence for Intercalation and Nucleic Acid Sequence Preferences. *Biochemistry* **1978**, *17* (23), 4845–4854.

(16) Friedman, A. E.; Chambron, J. C.; Sauvage, J. P.; Turro, N. J.; Barton, J. K. A Molecular Light Switch for DNA: Ru(Bpy)2(Dppz)2+. *J. Am. Chem. Soc.* **1990**, *112* (12), 4960–4962.

(17) Xiong, Y.; Ji, L.-N. Synthesis, DNA-Binding and DNA-Mediated Luminescence Quenching of Ru(II) Polypyridine Complexes. *Coord. Chem. Rev.* **1999**, *185–186*, 711–733.

(18) Bajaj, N. P. S.; McLean, M. J.; Waring, M. J.; Smekal, E. Sequence-Selective, pH-Dependent Binding to DNA of Benzophenanthridine Alkaloids. *J. Mol. Recognit.* **1990**, *3* (1), 48–54.

(19) Li, Z.-S.; Yang, H.-X.; Zhang, A.-G.; Luo, H.; Wang, K.-Z. pH Effects on Optical and DNA Binding Properties of a Thiophene-Containing Ruthenium(II) Complex. *Inorganica Chim. Acta* **2011**, *370* (1), 132–140.

(20) Medhi, C.; Mitchell, J. B. O.; Price, S. L.; Tabor, A. B. Electrostatic Factors in DNA Intercalation. *Biopolymers* **1999**, *52* (2), 84–93.

(21) Nieuwland, C.; Zaccaria, F.; Fonseca Guerra, C. Understanding Alkali Metal Cation Affinities of Multi-Layer Guanine Quadruplex DNA. *Phys. Chem. Chem. Phys.* **2020**, *22* (37), 21108–21118.

(22) Macii, F.; Cupellini, L.; Stifano, M.; Santolaya, J.; Pérez-Arnaiz, C.; Pucci, A.; Barone, G.; García, B.; Busto, N.; Biver, T. Combined Spectroscopic and Theoretical Analysis of the Binding of a Water-Soluble Perylene Diimide to DNA/RNA Polynucleotides and G-Quadruplexes. *Spectrochim. Acta. A. Mol. Biomol. Spectrosc.* **2021**, *260*, 119914.

(23) Biver, T. Discriminating between Parallel, Anti-Parallel and Hybrid G-Quadruplexes: Mechanistic Details on Their Binding to Small Molecules. *Molecules* **2022**, *27* (13).

(24) Malina, J.; Hannon, M. J.; Brabec, V. Recognition of DNA Three-Way Junctions by Metallosupramolecular Cylinders: Gel Electrophoresis Studies. *Chem. – Eur. J.* **2007**, *13* (14), 3871–3877.

(25) Duskova, K.; Lamarche, J.; Amor, S.; Caron, C.; Queyriaux, N.; Gaschard, M.; Penouilh, M.-J.; de Robillard, G.; Delmas, D.; Devillers, C. H.; Granzhan, A.; Teulade-Fichou, M.-P.; Chavarot-Kerlidou, M.; Therrien, B.; Britton, S.; Monchaud, D. Identification of Three-Way DNA Junction Ligands through Screening of Chemical Libraries and Validation by Complementary in Vitro Assays. *J. Med. Chem.* **2019**, *62* (9), 4456–4466.

(26) van Rixel, V. H. S.; Busemann, A.; Wissingh, M. F.; Hopkins, S. L.; Siewert, B.; van de Griend, C.; Siegler, M. A.; Marzo, T.; Papi, F.; Ferraroni, M.; Gratteri, P.; Bazzicalupi, C.; Messori, L.; Bonnet, S. Induction of a Four-Way Junction Structure in the DNA Palindromic Hexanucleotide 5′-d(CGTACG)-3′ by a Mononuclear Platinum Complex. *Angew. Chem. Int. Ed.* **2019**, *58* (28), 9378–9382.

(27) Zheng, S.; Siegler, M. A.; Roubeau, O.; Bonnet, S. Influence of Selenocyanate Ligands on the Transition Temperature and Cooperativity of Bapbpy-Based Fe(II) Spin-Crossover Compounds. *Inorg. Chem.* **2014**, *53* (24), 13162–13173.

(28) Thibault, M.; Luska, K.; Schlaf, M. An Improved Synthesis of 6,6'Diamino2,2'-Bipyridine. *Synth.-Stuttg.* **2007**, *2007*, 791–793.

(29) Swarts, A. J.; Mapolie, S. F. The Synthesis and Application of Novel Ni(Ii) N-Alkyl Dipyridylaldiminato Complexes as Selective Ethylene Oligomerisation Catalysts. *Dalton Trans.* **2014**, *43* (26), 9892–9900.

(30) Chachaty, C.; Pappalardo, G. C.; Scarlata, G. Molecular Conformation of Di-2-Pyridyl Sulphide. A Dipole Moment, 1H Nuclear Magnetic Resonance, and CNDO/2 Study. *J. Chem. Soc. Perkin Trans. 2* **1976**, No. 11, 1234–1238.

(31) Parks, J. E.; Wagner, B. E.; Holm, R. H. Syntheses Employing Pyridyllithium Reagents: New Routes to 2,6-Disubstituted Pyridines and 6,6′-Disubstituted 2,2′-Bipyridyls. *J. Organomet. Chem.* **1973**, *56*, 53–66.

(32) Canty, A.; Minchin, N. Synthesis of Symmetrical Poly(Pyridin-2-Yl)Ethane Ligands. *Aust. J. Chem.* **1986**, *39* (7), 1063–1069.

(33) Voisin, A. S.; Bouillon, A.; Lancelot, J.-C.; Lesnard, A.; Rault, S. Synthesis of Novel Halo-Oxybispyridines, New Building Blocks in Cholinergic Medicinal Chemistry. *Tetrahedron* **2006**, *62* (25), 6000–6005.

(34) Zhou, X.-Q.; Xiao, M.; Ramu, V.; Hilgendorf, J.; Li, X.; Papadopoulou, P.; Siegler, M. A.; Kros, A.; Sun, W.; Bonnet, S. The Self-Assembly of a Cyclometalated Palladium Photosensitizer into Protein-Stabilized Nanorods Triggers Drug Uptake In Vitro and In Vivo. *J. Am. Chem. Soc.* **2020**, *142* (23), 10383–10399.

(35) Zheng Xiaoyan; Chan Michael Ho-Yeung; Chan Alan Kwun-Wa; Cao Siqin; Ng Maggie; Sheong Fu Kit; Li Chu; Goonetilleke Eshani Chrisana; Lam William Wai Yan; Lau Tai-Chu; Huang Xuhui; Yam Vivian Wing-Wah. Elucidation of the Key Role of Pt···Pt Interactions in the Directional Self-Assembly of Platinum(II) Complexes. *Proc. Natl. Acad. Sci.* **2022**, *119* (12), e2116543119.

(36) van Rixel, V. H. S.; Siewert, B.; Hopkins, S. L.; Askes, S. H. C.; Busemann, A.; Siegler, M. A.; Bonnet, S. Green Light-Induced Apoptosis in Cancer Cells by a Tetrapyridyl Ruthenium Prodrug Offering Two Trans Coordination Sites. *Chem. Sci.* **2016**, *7* (8), 4922–4929.

(37) van Rixel, V. H. S.; Moolenaar, G. F.; Siegler, M. A.; Messori, L.; Bonnet, S. Controlling with Light the Interaction between Trans-Tetrapyridyl Ruthenium Complexes and an Oligonucleotide. *Dalton Trans.* **2018**, *47* (2), 507–516.

(38) Bonnet, S.; Siegler, M. A.; Costa, J. S.; Molnár, G.; Bousseksou, A.; Spek, A. L.; Gamez, P.; Reedijk, J. A Two-Step Spin Crossover Mononuclear Iron(Ii) Complex with a [HS–LS–LS] Intermediate Phase. *Chem. Commun.* **2008**, No. 43, 5619–5621.

(39) van de Griend, C.; van de Vijver, J. J.; Siegler, M. A.; Dame, R. T.; Bonnet, S. Ruthenium-Locked Helical Chirality: A Barrier of Inversion and Formation of an Asymmetric Macrocycle. *Inorg. Chem.* **2022**, *61* (40), 16045–16054.

(40) Addison, A. W.; Rao, T. N.; Reedijk, J.; van Rijn, J.; Verschoor, G. C. Synthesis, Structure, and Spectroscopic Properties of Copper(II) Compounds Containing Nitrogen–Sulphur Donor Ligands; the Crystal and Molecular Structure of Aqua[1,7-Bis(N-Methylbenzimidazol-2′-Yl)-2,6-Dithiaheptane]Copper(II) Perchlorate. *J. Chem. Soc. Dalton Trans.* **1984**, No. 7, 1349–1356.

(41) Martínez, C. H. R.; Dardonville, C. Rapid Determination of Ionization Constants (pKa) by UV Spectroscopy Using 96-Well Microtiter Plates. *ACS Med. Chem. Lett.* **2013**, *4* (1), 142–145.

(42) Kellett, A.; Molphy, Z.; Slator, C.; McKee, V.; Farrell, N. P. Molecular Methods for Assessment of

Non-Covalent Metallodrug–DNA Interactions. *Chem. Soc. Rev.* **2019**, *48* (4), 971–988.

(43) Shahabadi, N.; Kashanian, S.; Mahdavi, M.; Sourinejad, N. DNA Interaction and DNA Cleavage Studies of a New Platinum(II) Complex Containing Aliphatic and Aromatic Dinitrogen Ligands. *Bioinorg. Chem. Appl.* **2011**, *2011*, 525794–525794.

(44) Eriksson, M.; Mehmedovic, M.; Westman, G.; Åkerman, B. Time-Resolved Electrophoretic Analysis of Mobility Shifts for Dissociating DNA Ligands. *ELECTROPHORESIS* **2005**, *26* (3), 524–532.

(45) Malina, J.; Hannon, M. J.; Brabec, V. DNA Binding of Dinuclear Iron(II) Metallosupramolecular Cylinders. DNA Unwinding and Sequence Preference. *Nucleic Acids Res.* **2008**, *36* (11), 3630–3638.

(46) Long, E. C.; Barton, J. K. On Demonstrating DNA Intercalation. *Acc. Chem. Res.* **1990**, *23* (9), 271–273.

(47) Lippard, S. J. Platinum Complexes: Probes of Polynucleotide Structure and Antitumor Drugs. *Acc. Chem. Res.* **1978**, *11* (5), 211–217.

(48) McGhee, J. D.; von Hippel, P. H. Theoretical Aspects of DNA-Protein Interactions: Co-Operative and Non-Co-Operative Binding of Large Ligands to a One-Dimensional Homogeneous Lattice. *J. Mol. Biol.* **1974**, *86* (2), 469–489.

(49) Rocha, M. S. Revisiting the Neighbor Exclusion Model and Its Applications. *Biopolymers* **2010**, *93* (1), 1–7.

(50) Moura, T. A.; Junior, R. L. R.; Rocha, M. S. Caffeine Modulates the Intercalation of Drugs on DNA: A Study at the Single Molecule Level. *Biophys. Chem.* **2021**, *277*, 106653.

(51) McConnaughie, A. W.; Jenkins, T. C. Novel Acridine-Triazenes as Prototype Combilexins: Synthesis, DNA Binding, and Biological Activity. *J. Med. Chem.* **1995**, *38* (18), 3488–3501.

(52) Jana, P.; Šupljika, F.; Schmuck, C.; Piantanida, I. Naphthalene Diimide Bis-Guanidinio-Carbonyl-Pyrrole as a pH-Switchable Threading DNA Intercalator. *Beilstein J. Org. Chem.* **2020**, *16*, 2201–2211.

(53) Jones, D. C.; Hallyburton, I.; Stojanovski, L.; Read, K. D.; Frearson, J. A.; Fairlamb, A. H. Identification of a κ-Opioid Agonist as a Potent and Selective Lead for Drug Development against Human African Trypanosomiasis. *Biochem. Pharmacol.* **2010**, *80* (10), 1478–1486.

(54) Suh, D.; Oh, Y.-K.; Chaires, J. B. Determining the Binding Mode of DNA Sequence Specific Compounds. *Process Biochem.* **2001**, *37* (5), 521–525.

(55) Zhou, J.; Li, B.; Qian, Z.-C.; Shi, B.-F. Rhodium(III)-Catalyzed Oxidative Olefination of Picolinamides: Convenient Synthesis of 3-Alkenylpicolinamides. *Adv. Synth. Catal.* **2014**, *356* (5), 1038–1046.